8-1-1992

Design and evaluation of a screen-CCD imaging system for medical radiology

Jing Zhao

DESIGN AND EVALUATION OF A SCREEN-CCD IMAGING SYSTEM FOR MEDICAL RADIOLOGY

by

Jing Zhao

Center for Imaging Science
Rochester Institute of Technology

A Thesis submitted in partial fulfillment of the
requirements for the degree of Master of Science
in the Center for Imaging Science at the
College of Imaging Arts and Sciences
of the Rochester Institute of Technology

August 1992

Signature of the Author Jing Zhao

Accepted by Dana G. Marsh Sept. 25, 1992
Coordinator, M.S. Degree Program

COLLEGE OF IMAGING ARTS AND SCIENCES
ROCHESTER INSTITUTE OF TECHNOLOGY
ROCHESTER, NEW YORK

CERTIFICATE OF APPROVAL

M.S. DEGREE THESIS

The M.S. Degree Thesis of Jing Zhao
has been examined and approved by the
thesis committee as satisfactory for the
thesis requirement for the
Master of Science Degree

Dr. Zoran Ninkov, Thesis Advisor

Dr. Roger Easton Number Two

Dr. Thomas Morris Number Three

9/24/92
Date

THESIS RELEASE PERMISSION
ROCHESTER INSTITUTE OF TECHNOLOGY
COLLEGE OF IMAGING ARTS AND PHOTOGRAPHY

Title of Thesis DESIGN AND EVALUATION OF A SCREEN - CCD IMAGING SYSTEM FOR MEDICAL RADIOLOGY

I, Jing Zhao, hereby grant permission to the Wallace Memorial Library of R.I.T. to reproduce my thesis in whole or in part. Any reproduction will not be for commercial use or profit.

Date: 9/15/92

DESIGN AND EVALUATION OF AN IMPROVED X-RAY IMAGING SYSTEM FOR MEDICAL RADIOLOGY

by
Jing Zhao

Submitted to the
Center for Imaging Science
in partial fulfillment of the requirements
for the Master of Science Degree at the
Rochester Institute of Technology

ABSTRACT

A novel imaging system consisting of an X-ray source, an intensifying screen, optical coupling and a cooled CCD camera, for use in medical radiology was designed and evaluated, both theoretically and practically. Various characteristics of the system were analyzed and measured. It is concluded that the quality of images obtained with this system are comparable to or higher than those obtained using conventional systems.

ACKNOWLEDGEMENTS

I would like to acknowledge the following people for their help and support during this project.

Dr. Zoran Ninkov: for his guiding, helping and understanding.

Dr. Thomas Morris: for his help.

Dr. Peter D. Burns: for his help.

Dr. Rodney Shaw: for his help.

Dr. Mehdi Iravani: for his help

DEDICATION

For my wonderful family's hope, encouragement, support, and LOVE.

TABLE OF CONTENTS

Table of Figures

I. INTRODUCTION AND BACKGROUND

Since Roentgen's [1] discovery of X-rays, the multitude of phenomena observed when X-rays interact with matter has greatly enhanced our understanding of nature. The interactions of X-rays with matter and its dependence on atomic composition and density, in combination with the great penetrative power of X-rays, make up the basis for the application of X-rays as a diagnostic and constructive tool in the fields of medicine, science, and technology.

Various methods for viewing and recording of X-ray images have been used and continue to evolve, driven by the need for finer resolution and reduced patient dosage. Roentgen's discovery of X-rays and his initial experiments were made with a simple sheet of phosphorescent paper. This was refined into the fluoroscope: a luminous glass screen with a thin lead coating to protect the viewer from exposuring to the X-ray. Simultaneously, it was discovered that X-rays would create images directly on film, but that images were of relatively poor contrast, and required relatively high dosage. By combining the phosphor-coated paper or similar luminescent material now referred to as an intensifying screen, in contact with conventional light-sensitive film, better contrast can

be achieved at much lower dosage, but at the cost of image sharpness. With variations and refinements, this is the screen-film system still in use today. The screen-film technology is sufficiently mature that image quality is quite predictable, given well maintained equipment and a knowledgeable radiologist. However, by its nature, this method only affords static information and requires time to process the film, thus limiting the capability for real time analysis. In addition, the image must be digitized before computer enhancement techniques can be used. When operated above certain minimum exposure levels, the screen-film detector is fairly efficient, but improved image contrast is obtained at a cost of increased patient dose when a grid is used to limit X-ray scatter. Even the best obtainable film-screen resolution is not sufficient for certain applications, and is limited by the characteristics of commercially available films, such as the limited dynamic range, noise power at low and high spatial frequencies, and the base fog level. Other weak points of screen film system include the fact that film is not reusable, the film itself is costly due to the silver content, and the chemical bi-products of film manufacture are hazardous to the environment. Storage and retrieval of film can be difficult, particularly in a hospital setting.

In the recent past, image intensifiers also been used, both for direct viewing and recording with film and TV cameras. There are electronic or electro-optic devices used to create smaller, sharper, visible images. A prototype 2048 by 2048 pixel format digital radiography system with an image intensifier and TV camera has been developed, by Xonics Imaging, Inc.[2]. Unfortunately a characteristic of all radiographic X-ray systems

is that the original signal is degraded as several energy transformation stages are needed between X-ray generation and image recording. It would be desirable to avoid unnecessary energy conversion steps. American Science and Engineering was the first to use solid state detectors for high-resolution tomography [3]. Their approach was to convert X-rays into visible light in a scintillator crystal and image this light with a one dimensional linear EG&G Reticon photo-diode array. The major problem with this approach is that the linear array can only image one slice of the sample per measurement, thus scan times were quite long.

Charge Coupled Devices (CCDs), first introduced in 1970 by Bell Telephone Laboratories, possess characteristics of low noise, wide dynamic range, sensitivity, linearity, small pixel size and high charge storage capacity. They are available now at relatively low cost [24]. These advantages have resulted in increased use of CCDs in imaging applications.

A group at the Department of Radiology and the Optical Sciences Center at University of Arizona is developing a CCD-based system for application in coronary angiography [4][5]. The device consists of an external modular X-ray sensor, a proximity focused image intensifier and six CCD's coupled to the output of the image intensifier via six fiber-optic tapers. Three major problem areas which have been reported with this approach are: (a) distortion in the fiber optic tapers which were caused by defects in the fiber optic taper assembly; (b) field emission points and dead spots at the photocathode in the proximity focused image intensifier, and (c) light output of the

external sensors are reduced significantly because of coupling problems with the fiber-optic tapers.

To avoid these problems, this thesis reports on a novel system that directly images an intensifying screen, via an optical coupling lens, onto a 2025(H) by 2030(V) pixel full-frame CCD image sensor. This system is designed to avoid unnecessary energy conversion steps, limit distortion, and improve the modulation transfer function.

The high resolution radiographic imaging system discussed here uses a camera built around a KAF-4200 CCD array. The X-ray image is down converted to visible light using a phosphor coated intensifying screen, which is coupled to the thermoelectrically cooled KAF4200 by a lens. This system has the advantages of:

(a) detects and records the X-ray image electronically at high resolution;

(b) allows simple acquisition and real-time processing;

(c) allows easy archiving of the images for storage and later review;

(d) allows easy application of advanced techniques, such as: digital image enhancement, high speed data transmission, computer manipulation, high resolution CRT display, etc.

(e) low in cost over the long term compared to film-based systems.

In this thesis, the design of the overall system will first be described. Next, a theoretical analysis of the characteristics of the system, including signal to noise ratio, modulation transfer function, noise power spectrum (Wiener Spectrum), detective quantum efficiency and noise equivalent quantum, will be presented. Then, the laboratory experiments and results will be discussed. And finally, conclusions will be drawn and

suggested future improvements to this system will be presented.

II. APPROACH

i. SYSTEM DESIGN

The imaging system is shown in fig.1 and can be divided into a number of functional components: X-ray source, object (patient), intensifying screen, optical coupler, CCD camera, and computers. Beam from an X-ray tube penetrates a sample, and the transmitted radiation strikes an intensifying screen. The resultant fluorescent light is coupled to a thermoelectrically cooled CCD camera by a 50 mm Nikon lens. The images are stored on an IBM-compatable personal computer. Significant image processing in this prototype system is done off line on a SUN workstation. Each system component will now be discussed, along with the key factors of each which limit system performance.

Intensifying screen

As Fig. 1 illustrates, X-rays pass through a patient and strike an intensifying screen. Fluorescent light from the screen is coupled to the CCD camera by a lens, and digital images are acquired by the CCD camera. An intensifying screen reduces patient exposure by amplifying the signal when it converts the X-ray wavelength energy to visible light wavelength. However the screen degrades resolution by spreading the image of a point source of X-rays into a radial distribution of emitted light, thus limiting imaging resolution.

An intensifying screen is a composite of inorganic phosphor particles and organic

binder. X-rays are absorbed by high-z atoms in the phosphor and light is emitted [6]. The intensifying screen absorbs X-rays much more efficiently than silver halide film. A single X-ray is converted into as many as several thousand of visible photons [6] . The patient dose is minimized through reductions in exposure by factors between 30 to 800 [5].

The resolution of the final image is affected by many processes, but the principle limitation is from image spread in the screen, which is actually the result of two processes occurring in the intensifying screen as illustrated in Fig 2 [7]. These two processes are the deposition of X-ray energy, and the escape of the emitted light. These processes fundamentally limit resolution. If the energy of the incident X-ray is greater than the K-edge of the absorbing atom, a secondary X-ray may be emitted. If this secondary is then absorbed in another part of the screen, photons are generated at that point. Thus a single X-ray impact point may result in visible photons from a large area of the screen. Secondary emission is a random process, so some secondaries may be emitted almost parallel to the screen surface and travel a long way before being absorbed. Light emission is also a random process and a photon may be scattered many times before escaping from the screen.

Two other processes that affect resolution, but are of less concern:

1.) Compton scattering in the screen. Although there is Compton scattering in the screen, it is less than that generated in the patient. This scattering produces an X-ray background that limits the detectibility of low signal events.

2.) Emitted light may be absorbed by binder and/or the phosphor particles. This absorption can be deliberately increased by adding a dye. This absorption will increase resolution by preferentially eliminating photons which would otherwise emerge minimized.

In previous analysis, two facts have been determined. Firstly, X-ray energy spread can contribute to significant image spread. Secondly, light spread usually makes the larger contribution to image spread. All X-ray energy deposition is followed by light spread, but only a fraction occurs at secondary sites. Both light spread and energy spread increase with screen thickness.

To select an optimal intensifying screen for the system described here, a number of criteria were used. (a) a high X-ray absorption efficiency, (b) a high conversion ratio from X-ray photons to visible light, (c) a high emission efficiency (low self-absorption), (d) an emission spectrum closely matched to the wavelengths of maximum quantum efficiency for the CCD.

Kodak min R thin screen was chosen for this system. It has a good absorption and emission efficiency, and has a good spectral match to the KAF-4200 CCD camera compared with other screens available currently. Fig.3 shows the spectrum distribution of this intensifying screen.

Coupling lens

The lens acts as the optical coupling in this system between the fluorescent screen and detector. A high efficiency lens and highly efficient optical transmission are requirements in selecting a lens. High photon capture ability depends on a Numerical Aperture (N.A.), focal length and geometrical converting size.

A Nikon 50mm f/1.4 lens was chosen for this system.

CCD

A Photometrics CH-250 CCD camera was used for this system. The CCD camera used a Kodak KAF-4200 chip which was cooled using a three-stage thermoelectric cooler. The KAF-4200 is a high performance silicon charge-coupled device designed for a wide range of monochromatic image sensing applications in the 0.4μm to 1.1μm wavelength band [22]. The extremely low dark current (0.05 e^- sec^{-1} at -40C) of the KAF-4200 makes this device suitable for low light imaging applications. CCD cooling requirements, which are employed in the most demanding systems, are significantly reduced in this device since it can be operated in Multi Pinned Phase (MPP) mode [24]. The onchip output amplifiers have been specially designed to perform at a high speed operation (450MHz BW) at low noise levels (15e^- RMS) to increase frame rate. Total chip size is 19.1mm(H) by 19.8mm(V). The device characteristics are:

* Front illuminated Full-Frame Architecture,

reduced sensitive and interference effect

* 2025(H) by 2030(V) Photosensitive Pixels

* 9.0 μm(H) by 9.0 μm(V) Pixel Size

* 18.3mm(H) by 18.4mm(V) Photosensitive Area

* 100% Fill Factor

* Dual Readout Register

(only one is used in the Photometrics camera)

* Proprietary 2Φ Buried Channel Processing

* Additional On-Chip Dark Reference Pixels

* Low Dark Current (<10pA/cm^2 @ T=25c)

* High Dynamic Range (>72dB)

* High Output Sensitivity (10μV/e)

* Data rates up to 20MHZ/Register

* No Image Lag

Computer

Image acquisition and digitization (12-bit) were done in an electronics box located within 4 feet of the CCD head. Data is transferred to the control computer through a parallel cable. Clock patterns are generated using a Digital Signal Processor (DSP)-based custom card in the AT slot of the PC. The IBM PC has a 600 Mbyte hard drive for

temporary data storage and 17 Mbyte of RAM for real time display on a SuperVGA card. A SUN workstation is used for additional imaging processing and display. Data is transferred and archived via 8 mm tape cartridges. Each image occupies 8 megabytes of memory (2025 x 2033 x 2 bytes) in uncompressed form. Once the image is stored, the image can be digitally processed, manipulated, enhanced, filtered, displayed on CRT, printed, and archived on mass storage devices such as magnetic or CD discs. The images are displayed on a SUN monitor with the resolution of 1024 (H) by 900 (V).

ii. THEORETICAL MODELING

To evaluate the performance of this system, a theoretical model was used. Some characteristics were calculated based on typical values, approximate results were achieved to evaluate the quality and practicability of this system. The total system was divided into 10 steps and each characteristic associated with each step are discussed.

(a). GAIN

Referring to the schematic shown previously (Fig.1), there are at least eight stages in this system. The gain is calculated as a sequence of contributions from each stage as described below:

Stage 1 X-ray source emits X-ray photons. Mean number of X-ray quanta per unit area is q.

Stage 2 Intensifying screen absorbs X-ray photons. Absorption Efficiency η_a.

Stage 3 Intensifying screen converts X-ray photons to visible light quanta. Photon Gain m.

Stage 4 Intensifying screen emits light quanta. Emission Efficiency of light η_e.

Stage 5 Coupling lens collects emitted light. Numerical Aperture (N.A.).

Stage 6 Coupling lens transmits the light. Transmission of the lens τ.

Stage 7 CCD camera absorbs fluorescent photon, generates photoelectron. Quantum Efficiency η_{ccd}.

Stage 8 CCD collects electron, charge integration.

Stage 9 CCD transfers charge. The integrated charge is transferred from the sensor to charge-coupled device array.

Stage 10 On-chip output amplifier, and quantization.

The Mean Gain of the system is

$$G=\eta_a \bullet m \eta_e \bullet (N.A.)^2 \bullet \tau \bullet \eta_{ccd} \qquad (1')$$

$$G=\eta_a \bullet m \eta_e \bullet (N.A.)^2 \bullet \tau \bullet \eta_{ccd} \qquad (1')$$

The number of quanta received per pixel of the CCD is

$$Q_{ccd} = q \bullet A_e \bullet \eta_a \bullet m \bullet \eta_e \bullet (N.A.)^2 \bullet \tau$$

$$= q \bullet Ae \bullet G / \eta_{ccd} \qquad (1')$$

Where A_e is pixel size.

Thus the number of photoelectrons in CCD is

$$Ne = Q_{ccd} \bullet \eta_{ccd} = Q_{in} \bullet A_e \bullet \eta_a \bullet m \bullet \eta_e \bullet (N.A.)^2 \bullet \tau \bullet \eta_{ccd} \qquad (2')$$

Where according to the schematic Fig 1:

$$(N.A.) = \sin \alpha = (D/2)/(d_i^2 + D^2/4)^{-2} \approx D/2 \; / \; d_i$$

where D is the diameter of the lens.

Since

$$1/d_i + 1/d_c = 1/f \quad , \quad d_i/d_c = d_s/d_c \text{ and } F\#= f/D$$

where d_i is a distance between the screen and the lens, and d_c is a distance between the lens and the CCD. We get

$$1/d_i = (1/f) \bullet (d_{ccd}/(d_{ccd}+d_s))$$

so

$$(N.A.) = D \bullet d_{ccd}/2 \bullet f \bullet (d_{ccd}+d_s) = d_{ccd}/2 \bullet F^{\#} \bullet (d_{ccd}+d_s) \qquad (3')$$

Typical numbers of the parameters of this system [6]:

q=1mR=2.5x105 (X-ray photons/unit area), η_a=0.5, m=400 to 4000,

η_e=0.5, τ=0.8, η_{ccd}=0.3-0.6=0.3,

D=2"=2x25.4=50.8mm, f=1.4,

After substitute into Eq(2'), the number of photoelectrons of per pixel on the CCD is approximately:

$$N_e=2.5x105 \bullet 0.5 \bullet 1000.0 \bullet 0.5 \bullet [50.8 \bullet 18.4/2 \bullet 1.4 \bullet (18.4+254.0)]^2$$

$$\bullet 0.8 \bullet 0.3 \bullet 9.0x10^{-3} \bullet 18.4x10^{-3}$$

$$\approx 3730 \text{ (e-)}$$

The KAF-4200 CCD Image Sensor has high output sensitivity (10uv/e$^-$) [8]. The output voltage generated for the number of photoelectrons calculated above is

Vout = 10uv/e- x 3730.65e- = 37.3 mv

If fiber optic taper coupling were used instead of using optical lens coupling, the system efficiency would be [5]

$$N_t = Ne \bullet m_t^2$$

where m_t is the magnification of the fiber optic taper. This is a function of the size difference of both ends; in this case, m_t=3 to 5 [4].

(b). SIGNAL AND NOISE CHARACTERISTICS

The contributions to the signal to noise ratio are similarly caclulated for each stage as described below:

Stage 1: X-ray quanta emitted per unit area Qin.

Signal: $N1 = q$

Noise: $MSF1 = \sigma^2 = q$ (1)

MSF is mean square fluctuation. It is assumed that incident x-ray quanta are governed by Poisson statistics [23].

Stage 2: Screen absorbs X-ray quanta.

Signal: $N2 = q\eta_a$

Noise: $MSF2 = \sigma^2 = q\eta_a = N2$ (2)

Since the x-ray quanta are either absorbed or not absorbed by the intensifying screen, this absorption is a binomial selection process. The variance of η_a is $\sigma^2\eta_a=\eta_a(1-\eta_a)$.

Stage 3: m light photons are produced in the screen for each X-ray quantum absorbed.

Signal: $N3 = q\eta_a m = N2m$ (3)

Noise: $MSF3=\sigma^2=q\eta_a m+q\eta_a m^2\{1+\varepsilon/m\}$

$= N3 + N3m\{1+\varepsilon/m\}$ (4)

Where $\varepsilon=\sigma^2_m/m - 1$ is how much the variance exceeds m[18]. The relationship between the mean number of X-ray quanta per unit area q and the number of light photons produced per unit area N3 is expressed in Eq.(3). The statistics of X-ray quanta convertion to light photons was described by Swank [9]. The probability distributions are based on the characteristics of the scintillation spectrum of the phosphor. In a simplified case, if m is Poisson distribution $\sigma^2_m=m$, Eq. (4) will reduce to Eq. (5)

Special: $MSF3 = \sigma^2 = q\eta_a m(1+m) = N3(1+m)$ (5)

Stage 4: Photons produced in the screen are emitted in the proper direction with efficiency η_e.

Signal: $N4 = q\eta_a m\eta_e = N3\eta_e$ (6)

Noise: $MSF4 = \sigma^2 = q\eta_a(m\eta_e)^2\{1+\varepsilon/m\} + q\eta_a m\eta_e$

$= N4m\eta_e\{1+\varepsilon/m\} + N4$ (7)

The efficiency of photons emitted from the screen η_e is also binomial distribution, so $\sigma^2 = \eta_e(1-\eta_e)$. If according to Eq.(5)

Special: $MSF4 = q\eta_a m\eta_e(1+m\eta_e) = N4(1+m\eta_e)$ (8)

From Eq. (8), it can be concluded that the first term is the correlated noise due to the light photons produced from each X-ray quantum absorbed, since its variance is greater than that of uncorrelated photons ($\sigma^2 = N4$). The second term represents uncorrelated inherent photon noise, which must remain when all correlations among the photons are lost.

Stage 5: Emitted photons are collected by lens. The efficiency of light collection is given by the Numerical Aperture $(N.A)^2$ [4].
Here, $\eta_l = (N.A)^2$ is defined for simplicity.

Signal: $N5 = q\eta_a m\eta_e\eta_l = N4\eta_l$ (8)

Noise: $MSF5 = \sigma^2 = N5m\eta_e\eta_l\{1+\varepsilon/m\} + N5$ (9)

Collecting photons by the coupling lens is a binomial procedure, a light photon is either collected or it is not

$\sigma^2 = \eta_l(1-\eta_l)$.

Special: $MSF5 = N5(1+m\eta_e\eta_l)$

Stage 6: Coupling lens transmits photons, transmission τ.

Signal: $N6 = q\eta_a m\eta_e\eta_l\tau = N5\tau$ (10)

Noise: $MSF6 = \sigma^2 = N6m\eta_e\eta_l\tau\{1+\varepsilon/m\}+N6$ (11)

τ is binomial distribution, a light photon is either transmitted or not.

Special: $MSF6 = N6(1+m\eta_e\eta_l\tau)$

Stage 7: Photons are absorbed by the CCD, each absorbed photon generates a single electron-hole pair. At wavelength λ, the number of charges generated is described by the Quantum Efficiency of CCD, $\eta_{ccd}(\lambda)$ [22].

Signal: $N7 = q\eta_a m\eta_e\eta_l\tau\eta_{ccd} = N6\eta_{ccd}$ (12)

Noise: $MSF7 = \sigma^2 = N7m\eta_e\eta_l\tau\eta_{ccd}\{1+\varepsilon/m\}+N7$ (13)

The chance of a photon being absorbed by the photosensitive material can be described by a binomial distribution. A light photon is either absorbed leading to the generation of photoelectron or it is not, $\sigma^2 = \eta_{ccd}(1-\eta_{ccd})$

Special: $MSF7 = N7(1+m\eta_e\eta_l\tau\eta_{ccd})$

Stage 8: The electrons migrate to potential wells so that the collected charge represents the signal integrated in time over each photosite. The dimensions of the active pixel are Δx by Δy [10].

Signal: $N8 = \Delta x\Delta yN7 = q\eta_a m\eta_e\eta_l\tau\eta_{ccd}\Delta x\Delta y$ (14)

Noise: $MSF8 = \sigma^2 = \Delta x\Delta yN7$ (15)

The integrated pixel charge is Poisson distributed, because each variable is independently Poisson distributed. The spectrum shape of the integrated pixel charge remains unchanged since the pixel integration is over a nonoverlapping region, and the charge fluctuations are uncorrelated [11].

Stage 9: The CCD transfers the integrated charge from individual storage side through other storage site to the output amplifier.

Signal: $N9 = N8 = q\eta_a m\eta_e\eta_i\tau\eta_{ccd}\Delta x\Delta y$ (16)

Noise: $MSF9 = \sigma^2 = 4N\rho^2 N8$ (17)

Where ρ is a small fraction of charge lost during each transfer, N is the total number of transferred charges during the sampling interval. During each transfer over the length of the device, a small fraction ρ of the signal charge is left behind and is added to the next pixel charge. This introduces a source of image noise that blurs the image. Modern CCDs have a high charge transfer efficiency of about 0.9999, therefore the image degradation caused by this is assumed to be small enough to be safely ignored.

Stage 10: The on-chip circuitry consists of an output amplifier characterized by constant gain g, a linear filter which limits the output bandwidth, and an A/D converter which digitizes the result.

Signal: $N10 = N9g = q\eta_a m\eta_e\eta_i\tau\eta_{ccd}\Delta x\Delta y g$ (18)

Noise: $MSF10 = \sigma^2 = \Delta N^2(q)/12$ (19)

where $\Delta N(q)$ is the quantization interval written as a function of average input signal. For the special case of uniform quantization intervals, if N_{max} is the maximum pixel charge, b is the number of bits used in quantization, the variance is

Special: $MSF10 = \sigma^2 = N^2_{max}/12\ 2^{2b} = N10^2/12\ 2^{2b}$ (20)

According to Burns [11], there are three kinds of noise introduced by a CCD camera. Before this stage, the mean square fluctuation in the uniform image signal caused by quantum detection, photoelectron collection, and electron transfer is proportional to the mean signal. This

is referred to as shot noise. The second source of noise is fixed pattern noise, which results from pixel-to-pixel sensitivity variations in the device. Recently, several sources of fixed pattern noise have been reduced and can be further reduced by calibration and post processing. The other kind of noise is called read noise, and includes background noise, reset noise and output amplifier noise. They are combined uncorrelated with zero mean and variance. In stage 10, the output amplifier contributes an uncorrelated Johnson white noise component and a 1/f noise component. The number of bits used in quantization depends on the requirement of the imaging application, and is usually greater or equal to 8. In this system, 12 bits of quantization were used, for a total of 4096 quantization levels.

(c). SIGNAL TO NOISE RATIO

Signal-to-Noise Ratio (SNR) is an accepted method of describing the noise of a system or device in terms of either a particular signal level or the maximum usable signal level [13]. The signal and noise at each stage in this system were discussed above, so that the SNR can be derived by dividing signal characters by noise characters discussed before.

(d). MODULATION TRANSFER FUNCTION AND NOISE POWER SPECTRUM

The Modulation Transfer Function (MTF) is a useful and popular concept for describing the spatial resolving power of an X-ray image system because the MTF of a total system can be derived by simply multiplying the MTFs of its separate elements. The calculation of the MTF of system components is necessary to derive the MTF of the whole system.

The Noise Power Spectrum, or Wiener Spectrum, is the two-dimensional spectral density for a wide sense-stationary stochastic process [14]. It represents the decomposition of the variance of the noise over spatial frequency.

In this imaging system, before stage 4, (the light photons are produced in the intensifying screen), the noise of X-ray quanta is independent of spatial frequency. No other procedures change this white noise. The MTF due to scattering of X-ray quanta is too small compared to that of light photons to be considered.

When the light photons emerge from the intensifying screen, random scattering phenomena will affect the spatial frequency content. The light photon's distribution depends on the point spread function of this random scattering process [14]. If the MTF of the screen is expressed as $M_s(w)$, which is dominated by the effects of scattering of light photons within the screen, the Wiener Spectrum (noise power spectrum) of the light photons emitted from the intensifying screen can be described as

$$W1(u,v,q) = N_4 m \eta_e \{1+\varepsilon/m\} M^2_s(u,v) + N_4 \qquad (21)$$

$$MTF1(u,v) = M_s(u,v) \qquad (22)$$

Where $N4=q\eta_a m\eta_e$ as described before in Eq.(6). From this expression, it can be seen that only the correlated noise is affected by the random scattering. In stage 5 and stage 6, the noise spectrum of the light photon emitted from the screen becomes the input signal spectrum to the lens. The correlated noise component of Eq.(21) becomes signal modulation which will transfer through the modulation transfer function of the lens. The uncorrelated quantum noise component provides a part of the noise power spectrum of the lens. If $M_l(w)$ is the lens MTF for visible light exposures and $W_l(w,q)$ is the Wiener spectrum of the lens, the noise spectrum and MTF of this step are:

$$W2(u,v,q) = N_6 m\eta_e\eta_l\tau\{1+\varepsilon/m\}M^2_s(u,v)M^2_l(u,v) + W_l(u,v,q) \qquad (23)$$

$$MTF2(u,v) = M_s(u,v)M_l(u,v) \qquad (24)$$

In stage 7, the light photons emitted from the lens are absorbed by the photosensitive material of the CCD camera. The absorption of photons depends on the quantum efficiency $\eta(\lambda)$. There is no scattering associated with this absorption, so the spatial frequency is not affected, and the noise power spectrum W(u,v,q) and MTF(u,v) stay the same as Eq.(23) and Eq.(24). In stage 8, the photoelectrons are collected at each CCD pixel, and the diffusion of charge in the sensor is a source of image degradation. Charge diffusion is analyzed as an electron scattering process.

The MTF of this stage includes both the diffusion MTF $M_d(u,v)$ and the charge integration MTF. If the dimensions of the active pixel area are Δx and Δy, the integration MTF is $M_i(u,v)=\sin(2\pi u\Delta x)\ \sin(2\pi v\Delta y)/2\pi u\Delta x\ 2\pi v\Delta y$ [11]. During charge collection, the image signal is reduced, but the noise power spectrum remains the same. The MTF and noise power spectrum after charge collection are:

$$W3(u,v,q) = N6m\eta_e\eta_l\tau\{1+\varepsilon/m\}M^2_s(u,v) + W_l(u,v,q) \quad (25)$$

$$MTF3(u,v) = M_s(u,v)M_l(u,v)M_d(u,v)M_i(u,v) \quad (26)$$

In stage 9, the collected charges are transferred from an individual pixel to the output amplifier. During each transfer a small fraction ρ of the signal charge is left behind and add to the next pixel charge. This creates image blurring, and is a source of noise. If N is the total number of transfers and x is the effective image sampling interval for a simple readout scheme, the MTF of this transfer process can be expressed as $M_t(u) = \exp[-N\rho(1-\cos(2\pi ux))]$. If the noise power spectrum of charge transfer inefficiency is $W_t(u,v)$, the MTF and noise power spectrum of this stage can expressed as:

$$W4(u,v,q) = W3(u,v,q)M^2_t(u) + W_t(u,v) \quad (27)$$

$$MTF4(u,v) = M_s(u,v)M_l(u,v)M_d(u,v)M_i(u,v)M_t(u) \quad (28)$$

In stage 10, the on-chip amplifier amplifies the signal and also introduces an uncorrelated white noise and a 1/f spectral noise density to the read out noise. Given that the MTF of the amplifier is $M_a(u)$, the noise power spectrum of the readout noise created by the amplifier is $W_a(u,v)=(q_{max}/DR)^2M^2_a(u)$, where DR is the dynamic range of the CCD camera defined as DR=saturation signal/RMS pixel dark noise. There is another noise source caused by digital quantization in the A/D converter, with noise power spectrum $W_q(u,v)=N^2_{max}/12\ 2^{2b}$, where N_{max} is the maximum number of electrons that can

be stored in a pixel before saturation, and b is the number of quantization bits used (greater than or equal to 8 for image applications). The MTF and noise power spectrum after this stage give a noise power spectrum and system MTF of:

$$W(u,v,q) = [W4(u,v,q) + W_a(u,v)]M^2_a(u) + W_q(u,v)$$

$$= [N6m\eta_e\eta_i\tau\{1+\varepsilon/m\}M^2_s(u,v)+W_i(u,v,q)]M^2_t(u)+W_t(u,v) + W_a(u,v)\}M^2_a(u) + W_q(u,v) \quad (29)$$

$$MTF(u,v) = M_s(u,v)M_i(u,v)M_d(u,v)M_i(u,v)M_t(u)M_a(u) \quad (30)$$

(e). DETECTIVE QUANTUM EFFICIENCY AND NOISE EQUIVALENT QUANTA

In an ideal (perfect) imaging process, the actual and predicted MTFs will be identical, but for all practical cases where noise is introduced or enhanced during imaging, the ratio of MTF(practical)/MTF(ideal) is less than 1, and this ratio is widely known as the Detective Quantum Efficiency (DQE). We can think of an imaging process as a "black-box" operator in the S/N sense

$(S/N)^2_{in}$------- DQE ------ $(S/N)^2_{out}$

IMAGING PROCESS

By definition $(S/N)^2_{out}$ has an upper limit of q_{in}, and for an ideal imaging process, or detector $(S/N)^2_{out} = (S/N)^2_{in}$. For all practical cases where noise is

introduced or enhanced, $(S/N)^2_{out}$ is less than q_{in} by a multiplier fraction which is the DQE. $(S/N)^2_{out}$ is the noise equivalent number of quanta (NEQ). It can be viewed as an imaging process which had attempted to count q_{in} quanta but was only successful in counting NEQ of them. Alternately it may be thought of as the lower exposure level. An ideal detector would have needed to achieve the same S/N in the output.

$$NEQ = (S/N)^2_{out} = q_{in}DQE$$

The concept of NEQ provides a nice measure of the output image quality which is independent of the signals which are conveyed with these quanta. The DQE for an imager can be expressed by:

$$DQE(w,q) = q\, G^2MTF^2(w)/W(q,w) \qquad (31)$$

where G is the mean gain of the system. This was calculated previously in Eq.(1). MTF and W are the Modulation Transfer Function and Wiener Spectrum of the system.

Eq.(1), Eq.(29) and Eq.(30) can now be substituted into Eq.(31) to express the DQE of the system:

$$DQE(w,q)=\frac{q[\eta_a m\eta_e(N.A.)^2\tau\eta_{ccd}]^2[M_s(w)M_i(w)M_d(w)M_i(w)M_t(w)M_a(w)]^2}{[N6m\eta_e\eta_i\tau\{1+\varepsilon/m\}M^2_s(w)+W_i(w,q)]M^2_t(w)+W_t(w)+W_a(w)\}M^2_a(w)+W_q(w)} \qquad (32)$$

$$NEQ(w,q) = qDQE(w.q) \qquad (33)$$

(f). SAMPLE CALCULATION

SIGNAL vs EXPOSURE

The final signal of the CCD can be expressed as the number of photoelectrons. According to Eq.(2'), the relationship of signal and exposure is linear before saturation. Fig.4 shows a plot of the number of output e^- on the CCD vs. X-ray photon irradiance.

GAIN vs F#

From Eq.(1'), it is seen that the Mean Gain is a function of second power of Numerical Aperture of the lens. Since Numerical Aperture is inversely proportional to the F#, which is expressed in Eq.(3'), as the F# varies, the gain of the system changes. Figure 5 shows the change of the mean gain of the system as a function of the F# of the lens and M (the ratio of the width of the full CCD chip and that of the intensifying screen). Fig.5.1 to Fig.5.5 shows gain vs F# at M=0.1, 0.3, 0.5, 0.7, and 0.9.

MODULATION TRANSFER FUNCTION &

WIENER SPECTRUM vs EXPOSURE & FREQUENCY

The system MTF is the product of the MTF of the screen, lens, and CCD including charge diffusion, integration, transfer and amplifier procedures. The MTFs of the intensifying screen and the lens were plotted in Figure 6 and Figure 7 respectively. The 1-D diffusion MTF is assumed to be of Gaussian shape [11], and the integration MTF is given by Eq.(25). Since the industry standard for charge transfer efficiency is greater than 0.99999 for modern CCDs, we assume M_t=1. The amplifier MTF is described by a low-pass filter:[11]

$$M_a(w) = 1/(1+w/7)$$

where w is angular frequency, so the MTF of the CCD was computed and plotted in Figure 8. The combined system MTF is shown in Figure 9.

The noise power spectrum of the system is described by Eq.(29). The W of the lens is assumed to be a normal distribution. Because the high efficiency of charge transfer, W_t=0. The amplifier noise power spectrum is:

$$W_a(w)=(N_{max}/DR)^2M^2_a(w)=225M^2_a(w) \text{ electrons}^2/\text{pixel}$$

where for this CCD camera, N_{max}=85000 electrons, DR=85000/15=5667.

For uniform quantization, SNR is defined as SNR = $12^{-2}\bullet 2^N$, where N = bits of quantization. If 12 bits are used, the spectrum of the quantization noise is: [11]

$$W_q = N^2_{max}/(12\bullet 2^{2b}) = 85000^2/(12\bullet 2^{24}) \approx 36 \text{ electrons}^2/\text{pixel}$$

The result of the noise power spectrum combination is shown in Figure 10.

DQE & NEQ vs EXPOSURE & FREQUENCY

The DQE & NEQ were discussed before and the expressions were derived at Eq.(32) and Eq.(33) respectively. With all the assumptions listed above, the system's DQE and NEQ are computed and shown in Figure 11 and Figure 12.

iii. EXPERIMENTAL MEASURING

An evaluation of the imaging system was made by measuring and studying different imaging characteristics. The ideal image evaluation test should be accurate and able to determine the quality of the imaging system. Measures of image performance such as resolution or modulation transfer function, noise power spectrum, contrast, and signal-to-noise ratio were used for evaluation of the imaging system.

SYSTEM SET UP

The imaging system configuration for this evaluation is show in Fig.13. The X-ray source was provided by the Radiology Department of the University of Rochester, and consists of Mo with 1mm Al filter. The intensifying screen (Min-R fast screen) was provided by the Health Science Research Department of Eastman Kodak. The lead glass was of RD-50 type, set to absorb X-ray photons that penetrated the fluorescent screen, and thus prevent them from striking the CCD [15]. It is known that such impacts can degrade the performance and lifetime of the chip. An 8 x 10 camera frame was used to mount the screen and CCD, and to provide isolation from room light. Originally a 50mm f/1.4 lens was to be used, but the focal length adjustment was limited by the 8 x 10 frame, so a 50mm f/2.8 lens was used instead for these measurements. A 386 PC with 17MBytes RAM was used for acquiring images. Data was stored on 8mm tape. All images were later processed and analyzed on a SPARC 2 SUN workstation at the Center for Imaging Science at the Rochester Institute of Technology.

RESOLUTION TEST

The resolution measurements were performed for variations in energy and exposure time. A standard tri-bar resolution tile was attached to the front of the intensifying screen between the screen and X-ray source. The tile is constructed using parallel lead bars with different widths. X-ray voltage increased from 40kVp to 80kVp in 10kV intervals, whilst images were taken and stored consecutively. Then while holding the X-ray voltage at 60 kVp, seven images were acquired whilst changing the X-ray exposure time from 30ms to 2 seconds with double increments. During this procedure, the camera exposure time had to be changed to encompass the X-ray exposure time. For all the measurements, the X-ray exposure current was set at 500mA.

Four images were chosen to be used to derive the MTF. They were: image 1 taken at 60Kv, 500mA and 100ms, image 2 taken at 60kv, 500mA and 200ms, image 3 taken at 25kv, 500mA and 100ms, and image 4 taken at 25kv, 500mA and 2s.

The images were analyzed on the SUN workstation, and the relationship of resolution vs X-ray voltage (energy) and resolution vs exposure time (flux) were measured and plotted. They are shown in Fig.14 through Fig.17.

The MTF of the system was obtained by measuring the edge function, computing its derivative, and performing DFT (Discrete Fourier Transform) calculation as plotted in Fig.18.

The MTF values of these measurements for different imaging conditions could also be obtained from measured Line Spread Function (LSF) data. The MTF is obtained from the histogram of the LSF, S(I,z) using the method described by MacIntyre, et al [16] from the incremental readings I in a direction perpendicular to the line source. If there are a total of M points in the LSF measure and Δw is the increment in frequency

then:

$$MTF = \frac{\sum S(I,z)\cos^2[2\pi\Delta v(N-1)\Delta x(I-(M+1)/2)]}{\sum S(I,z)}$$

where S(I,z) is the value of the line spread histogram at Δx [I-(M+1)/2] and $w = \Delta w(N-1)$.

CONTRAST TEST

Contrast of each image was measured by reading the maximum and minimum counts listed in the Table 1.

Contrasts of resolution of 4 lp/mm of tri-bar images taken at different conditions were measured and can be compared in Table 2.

The contrast test was done by using an arterial phantom which has a construction of 8 parallel cylindrical tubes of differing diameters filled with iodine in a 25mm thick lucite plate. The contrast details were determined by the percentage of the signal value at the arterial lines and the original signal value. Fig.19 presents the contrast curve for this test. The contrast test could be done more easily using a standard contrast detail phantom. An arterial phantom was chosen so that an additional measure of the quality of the imaging system for arteriography could also be made.

SIGNAL TO NOISE RATIO

There were five sets of images taken in the same experimental environment; no object, rabbit liver section, tri-bar object, phantom with tri-bar, and phantom with arteries. Each set was taken with varied X-ray energy voltages, but the same exposure time, and with varied exposure times but the same voltage.

Signal-to-noise ratio of the tri-bar image at 60kV, 500mA and 100ms exposure time was obtained by using IRAF [19] software on the SUN workstation, plotting the signals of rows for different resolutions, average signals and average noises were read and calculated and shown in Fig 20.

Signal-to-noise ratios of tri-bar images taken at the same voltage, same intensity different exposure times is shown in Fig.21. Comparison of the relationship of SNR with exposure time at different exposure energy is shown in Fig.21 and Fig.22.

ATTENUATION MEASURE

A block of phantom was attached to the intensifying screen, a resolution tile was attached to the center of the phantom, and three images were taken at X-ray tube voltages of 25kV, 500mA with exposure times 1/5 sec, 1 sec and 2 sec, respectively. Signal-to-noise ratios were measured and listed in Table 2. According to Beer's Law, $S = S_0 e^{-\mu t}$ [17], where S_0 is the original signal, S is the final signal, t is a thickness of the material, and μ is the attenuation coefficient. The thickness of the phantom is 2cm, so the attenuation of the material of the phantom could easily be calculated.

CLINICAL USE

In order to evaluate images of a real object, a rabbit liver section was provided by the Radiology Department of the University of Rochester. A slice of sample about 1cm thick was taken used to observe the practicality of the system. Two images of the sample were taken with 50kV, 500mA, 2sec and 25kV, 500mA, 2sec conditions. The images are shown on Fig.23 and Fig.24.

III. RESULT AND DISCUSSION

The results of the theoretical modeling and experiments illustrate the most important features of the system.

Fig.4 shows the relationship of X-ray exposure photon and final electrons per pixel based on the typical parameters which were listed before. The system is linear with gain (which is the slope of the line) of 0.015, so the efficiency of signal transfer is about 1.5%. From Eq.(1'), it can been seen that the gain is the result of multiplication of the gain from each stage. The main limitation comes from the Numerical Aperture (N.A.) of the lens, and from Eq.(3'). The N.A. is proportional to the ratio of the size of the CCD and the screen and is inversely proportional to the F# of the lens, so the gain can be increased for the right combination of F# and sizes of the screen and CCD. The emitting efficiency curve of the intensifying screen does not correlate well with the spectral response curve of the CCD. This can be seen from Fig.3 and Fig.22. This is another reason for decreased system efficiency. It was very difficult to find an intensifying screen whose peak emission wavelength is above 650nm, but the peak spectral response of the KAF4200 CCD camera is around 700nm. To improve this factor, more research in the chemical coating materials area needs to be explored.

Since the saturation level of the CCD is 85000 e^-/pixel, the maximum X-ray exposure is about 5.67×10^6 X-ray photons/pixel, so for clinical use, usually the exposure is less than 10^5 X-ray photons/pixel, so it is well below the saturation limit of the CCD. Another way to avoid damaging the CCD camera is to place a piece of lead glass behind the screen. The lead glass used in the test is 10mm thick (lead equivalent x=3.2mm), the attenuation coefficient of lead is $100cm^-$, the number of X-ray photons

compared to that before is $N/N_0 = e^{-\mu x} = e^{-100x0.32} = 1.27x10^{-14}$. Thus almost all the X-ray photons penetrating the intensifying screen are absorbed by the lead glass.

Fig.5 shows the plot of the system Gain vs F# and M, where F# is the focal length of the coupling lens divided by the diameter of the lens, and M is the ratio of the CCD detector to the size of the intensifying screen. For each curve in Fig.5, it can be seen that as the F number increases, the total gain of the system decreases. As the F number is reduced, the gain rises steeply. This is because the total gain is a function of the second power of the F#. If M is constant,from 0.1 to 0.9 interval 0.2, then pick one of the plots among Fig.5.1 to Fig.5.5, selecting an F# corresponds to a certain gain of the system. If F# is already decided, on Fig.5, vertically each F# has five sets of gains corresponding to different M values, the higher the M values, the larger the gain. That means the size difference between the intensifying screen and CCD's active pixel area contributes to the system gain. The larger the pixel size, the better the optical coupling and the higher the gain. The F# and the M of the system were designed for 1.4 and 0.36, but the F# of the lens used for taking the images presented here was 2.8. This was because of the problem focusing with the limited mechanical mount available. Thus the gain of that system is only one fourth of the one designed, reducing the quality of the images.

Fig.6 to Fig.8 are the MTFs of the CCD, lens and screen respectively. The cutoff frequencies (defined as MTF=0.1) are: 52 cycle/mm for the CCD, 6 cycle/mm for the lens, and 10 cycle/mm for the screen. Fig.9 shows the theoretical MTF of the system according to the Eq.(30). It is the product of the MTFs of each of the separate components. The 10% cutoff frequency of the system's MTF is about 5.6 cycle/mm.

Fig.10 is the plot of the Wiener Spectrum of the system according to

Eq.(29). It is the function of both exposure and frequency, the higher the exposure and frequency, the larger the Wiener Spectrum. The value of the Wiener Spectrum of this system is in the range of ten to the fourth power.

Fig.11 and Fig.12 are the DQE and NEQ of the system according to Eq.(32) and Eq.(33). The highest DQE is about 75% at a certain combination of exposure and frequency value, when the frequency or exposure is above that value, the noise increases, thus the detective quantum efficiency decreases. NEQ shows how good the quanta acquisition of the imaging system is, it is also a function of the exposure and frequency. This has a similar shape to the DQE surface. From Fig.12, the value of the NEQ is in the range of ten to the fifth power, which is close to the NEQ value of the conventional screen film system.

Fig.14 to Fig.17 are the measured and calculated MTFs of the system at different exposure conditions. If one compares Fig.14 with Fig.15, and Fig.16 with Fig.17, it shows two set MTFs at the same exposure energy(kV) and intensity(mA), but with different exposure times. Both sets showed the MTF increasing with longer exposure time. At the lower voltage (Fig.16 and Fig.17 25kV), the difference in MTFs using different exposure times is smaller than that of the higher voltage. At high voltage, when the exposure time decreases, the MTF drops quickly, but for low voltage exposures, such as used in mammography, low dosage does not affect the resolution of the image significantly [21]. This may be a significant advantage with the known higher risk of getting cancer with larger dosage. If one compares Fig.14 with Fig.17, it shows the MTFs of the system with the same exposure intensity and same exposure time but different exposure energy. At low frequency, the MTF of both are similar. When the voltage is lower, the MTF is a little higher, but when the frequency increases, the MTF

of the high voltage exposure drops fast. So, at high frequency, the MTF of the low exposure energy is higher than that of the high exposure energy. To get high resolution, the user can either use the lower voltage with longer exposure time, or high voltage with shorter exposure time, the choice depends on the application.

From those four figures, it can be seen that the limiting resolution of the system is between 7 cycle/mm to 8 cycle/mm. For 10% MTF cutoff, frequencies are between 4 cycle/mm to 5 cycle/mm. Several limitations and potential improvements are discussed below:

The system resolution is limited primarily by the MTF of the lens. With the optical fiber taper coupling, the system's MTF is expected to approach an increase of approximately 25%. The MTF of the intensifying screen will be the primary limitation for the system if a fiber optical taper is used to couple the light. The highest quantum efficiency value of intensifying screens available happens at green or blue light wavelength, but the peak value of the quantum efficiency of the CCD is near red light wavelength. If a red emitting screen were available, the efficiency of the system would increase. To obtain the same MTF, lower dosage would be used or the same dosage would give a better MTF.

Focusing is another factor needing to be improved, since the focal spot size effects the MTF of the system. Focusing the lens of this system before taking images was done by adjusting the screen back and forth to get the best reference image. Error in focusing can be attributed to personal judgement. If there is an auto focusing system installed within the system, the resolution will be significantly improved.

When the images were taken, there was some room light coming into the system, which reduced the resolution of the images. The measured MTF is lower as a result than

the system without the glare would have been.

Most CRTs cannot display the large dynamic range and resolution of the CCD, so even though the CCD image has high resolution, when it is displayed on a CRT, the resolution is limited by the pixel range of the CRT. For this project, the images were transferred to SUN workstation, and the resolution of the monitor of the workstation was only 1152 by 900 pixels. This is better than most PC monitors, but still substantially less than the 2K by 2K images acquired by the CCD.

Error in measurement is another important limitation in determining the MTF of the system. Reading of gray values to get the edge function, and DFT (Discrete Fourier Transform) of the derivative of the edge function, will introduce numerical errors. Repeating the measurement and averaging the result will reduce the error.

Fig.20 to Fig.22 are the Signal to Noise Ratio (SNR) of the system measured under different conditions. Fig.20 is the SNR at each resolution of the image taken at the clinical condition, 60KV, 500mA and 100ms exposure time, when the resolution increases, the SNR decreases. After 4 cycle/mm, the SNR drops rapidly. Fig.21 and Fig.22 shows the relationship between SNR and exposure time at both low voltage (25KV) and high voltage (60KV) exposure. At high voltage, SNR decrease gradually when the exposure time increases. At low voltage, the relationship is opposite. SNR increases when the exposure time increases. As shown in Fig.20 and Fig.21, lower exposure voltage provides higher SNR. Fig.19 is the result of the contrast test. As $S=S_0e^{-\mu t}$ demonstrates, it should be logarithmic. Since the difference of the depth is very small, and the depth is very shallow, the contrast of the arteries and the background is very small, and the image quality is relatively poor, it was difficult to measure the relative contrast. This affected the accuracy of the curve, but the tendency still can been seen.

Fig.24 to Fig.28 are prints of rabbit liver section and tri-bar tile images taken at the Research Department of Radiology at the University of Rochester. Table 3 contains basic statistics of these images.

Fig.24 is the image of a rabbit liver section.

It was taken at 50 KV, 500mA and 500 ms.

Fig.25 is the image of a tri-bar tile by itself.

It was taken at 60 KV, 500mA and 100ms.

Fig.26 is the image of a tri-bar tile,

It was taken at 25 KV, 500mA and 100ms.

Fig.27 is the image of a tri-bar tile attached on a piece of lucite block that was 1 inch thick. It was taken at 25 KV, 500mA and 200ms.

Fig.28 is the image of arteries etched in a pixel of lucite block that was 1 inch thick. It was taken at 25 KV, 500mA and 2sec.

Table.3 is statistics of images measured by IRAF.

IV. CONCLUSION AND RECOMMENDATION

A design and evaluation of an imaging system for medical radiology was the goal of the project. Based on the theoretical analysis, modeling, experimental measurments, and processing, it appears that a system composed of an intensifying screen, optical coupling and high resolution CCD camera is indeed an imaging system capable of taking high quality radiographic images. In addition, it allows easy imaging processing, and greatly improved file management. As discussed, the characteristics of the system are high efficiency and spatial resolution, and low noise. The system is comparable to or better than the conventional screen film system now in use [20].

For screen film systems, light capture efficiency of the screen is about 30%, light collection effiency of film is about 100%, and the DQE of film is about 20%, so the total efficiency (gain) of the system is about 6%. For this system, light capture efficiency of the screen is also assumed to be about 30%, light collection of the lens is about 80%, the numerical aperture of the lens is about 1.2, and the quantum efficiency of the CCD is about 30%, so the total efficiency is about 11%. This system has greater overall efficiency than screen film systems.

The MTF of screen film system varies in accordance with source wavelength, thickness of screen coating, and the type of film used, but the cutoff frequency of MTF=0.1 is between 6 to 10 cycle/mm [18]. The cutoff frequency of MTF=0.1 of this system is about 7.8 cycle/mm, so the resolution of this system is similar to some screen film systems, and better than others.

The DQE of the CCD is higher than film [6][14]. The DQE of screen film systems is below 40%, usually about 20%, while the DQE of this system at most frequencies is above 20%, so the DQE of this system is higher than most screen film systems.

The CCD has low noise and wide dynamic range characteristics. All films have fog noise, and some have limited dynamic range. The signal to noise characteristics of this system are comparable to or better than screen film systems.

CCD based systems of this type have exciting applications in digital X-ray imaging, and can also be applied to the areas as diverse as tomography, crystallography, topography, and manufacturing inspection.

This project is limited by the available time and funds. If it were possible, there are several improvements that could be made. Increasing the intensity of X-ray sources, finding a better intensifying screen, changing the optical coupling method by using a fiber optical taper, and designing and installing an auto-focus system will significantly improve the characteristics of the system. A variety of additional image processing procedures could be applied to the data to improve the quality of the images and more measurements could be made, to allow more precise conclusions to be drawn.

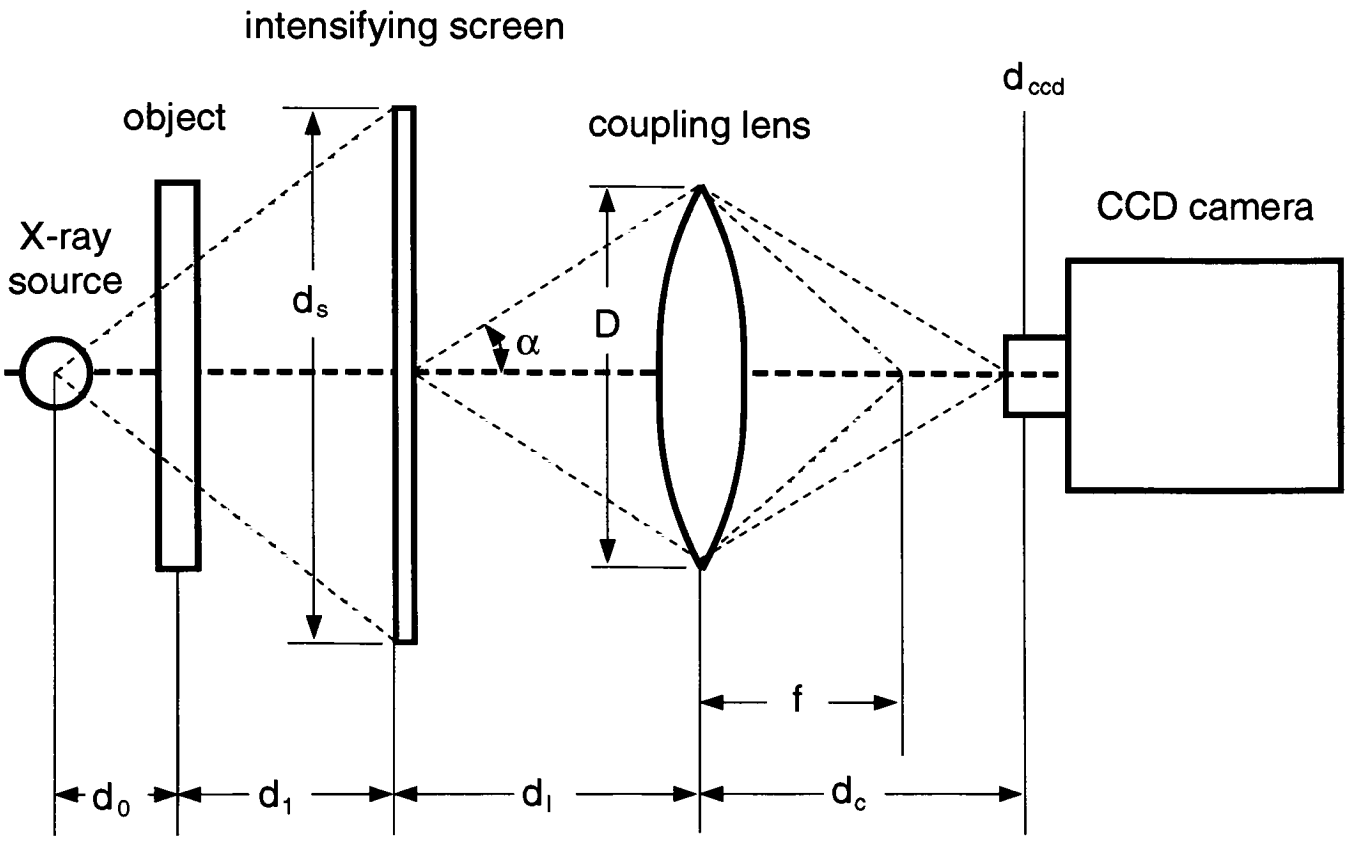

Fig.1 The system can be divided into a number of functional sections: X-ray source, object (patient), intensifying screen, lens, CCD camera, and computer processing center.

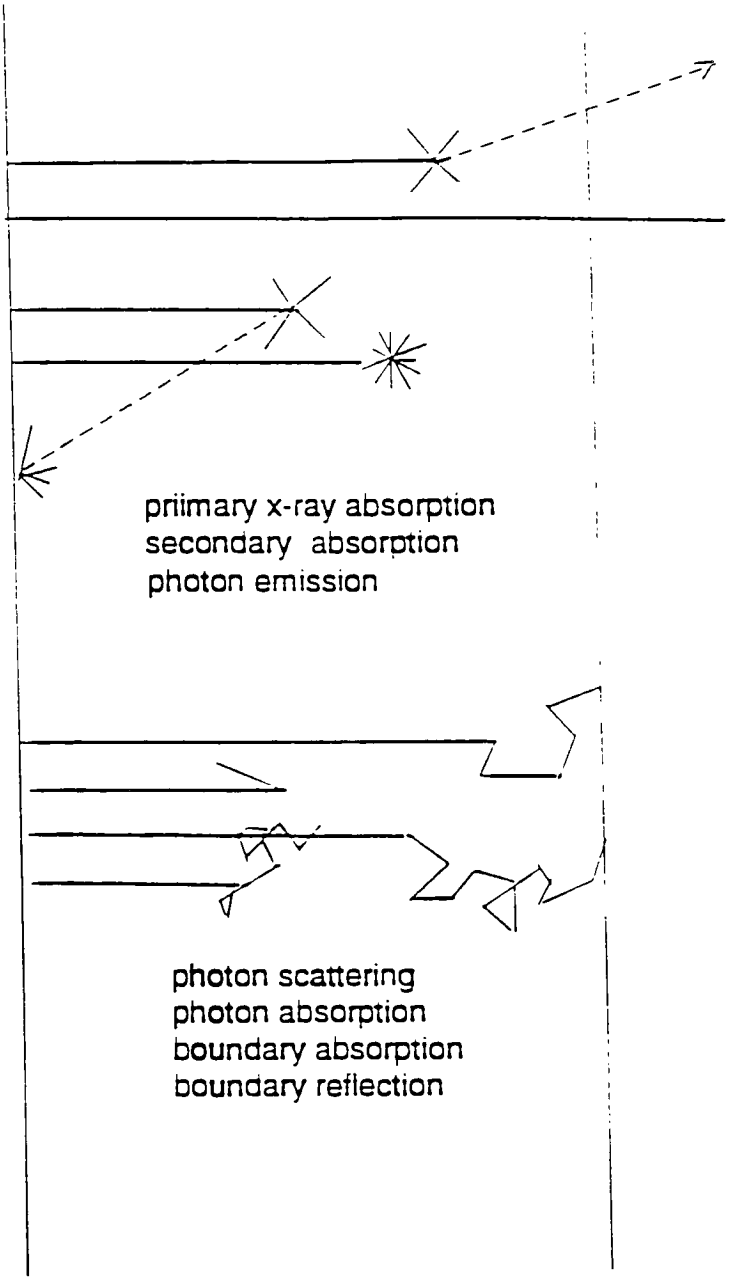

Fig.2 X-ray absorption and photon transport processes occuring in an X-ray intensifying screen.

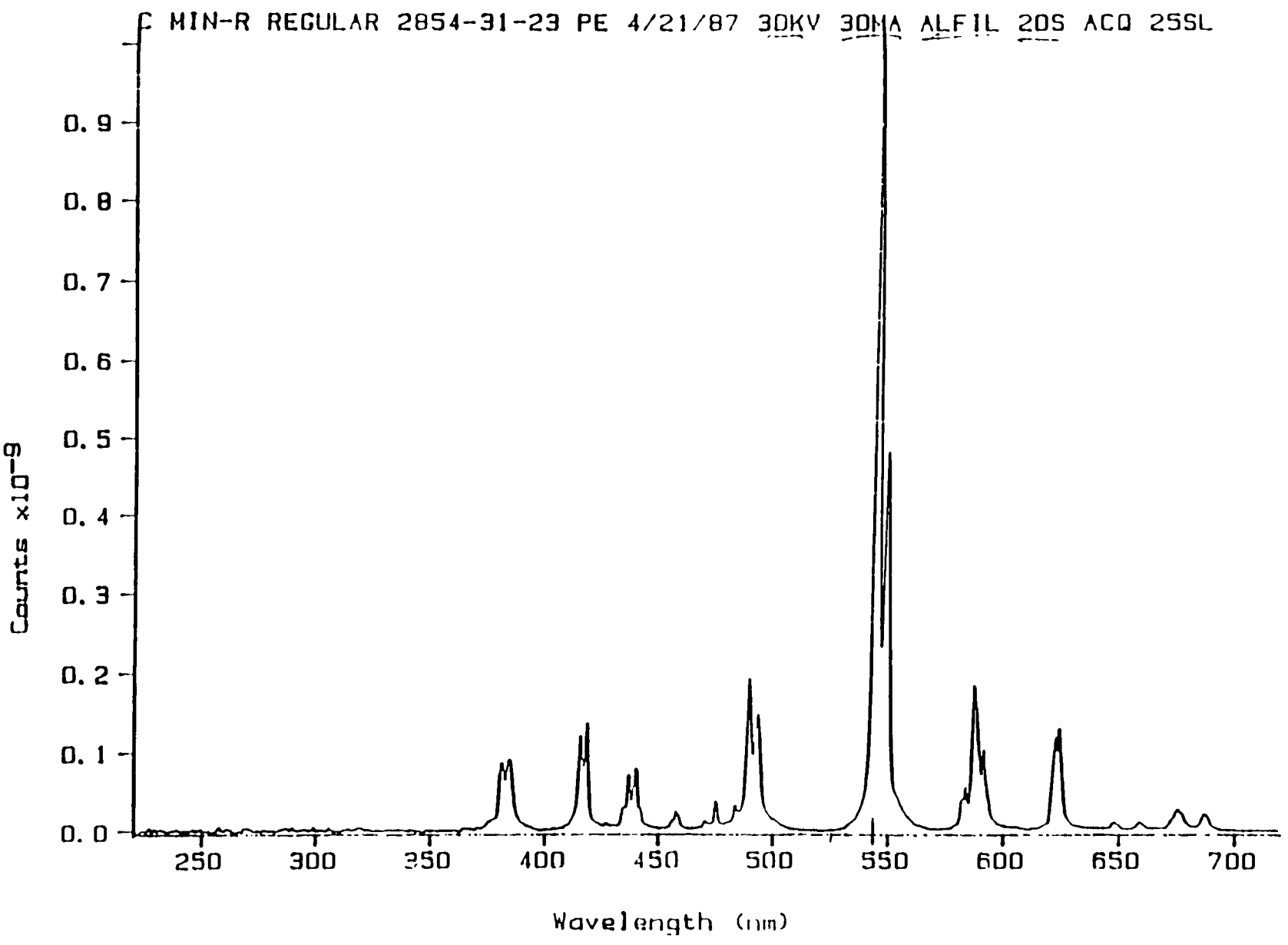

Fig.3 Spectrum distribution of Min R screen. It has a better spectral match to the KAF-4200 CCD camera than other available screens.

Fig.4 Signal vs. Exposure

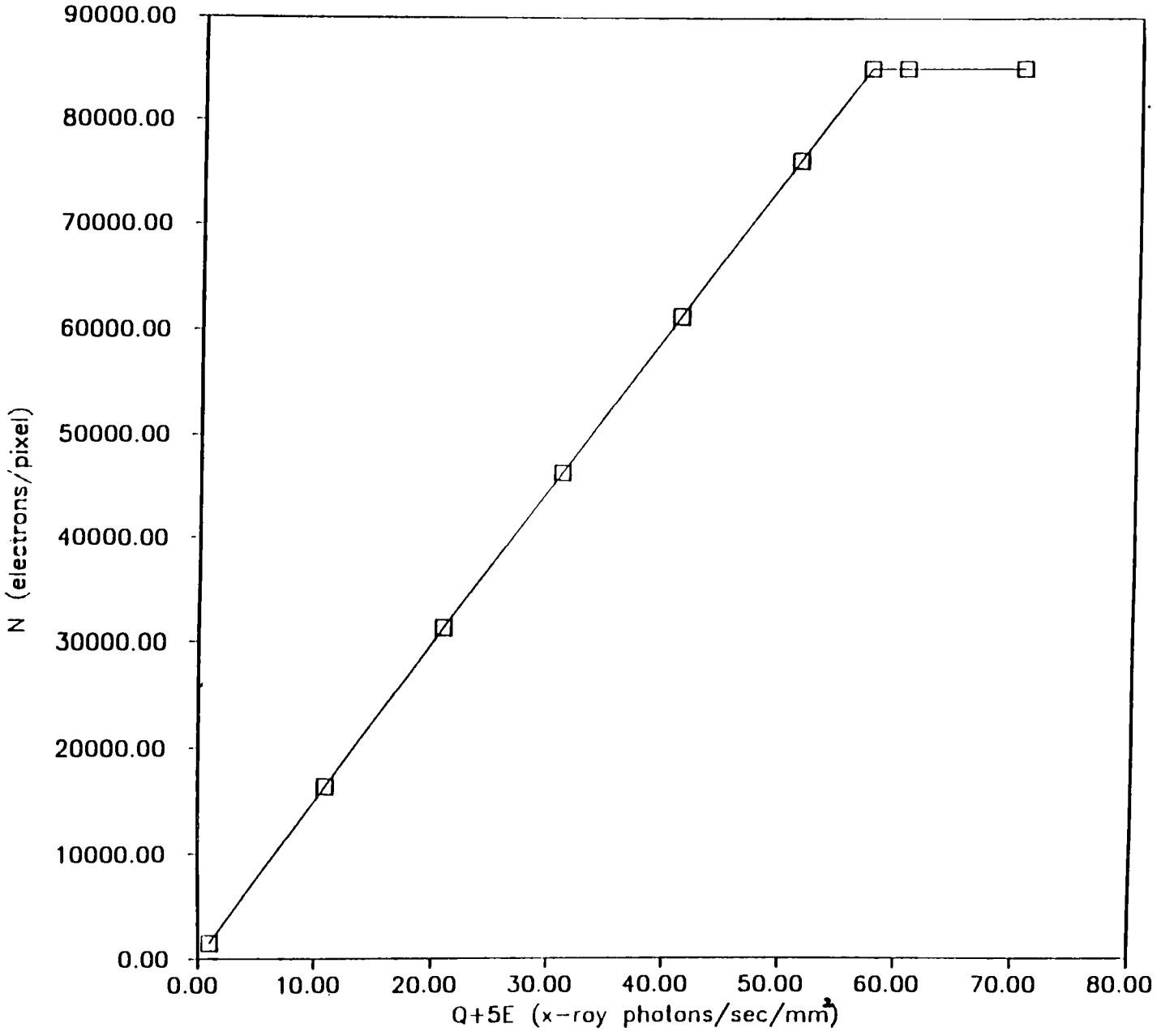

Fig.4 The relationship of the signal from the CCD and the X-ray flux on the intensifying screen is linear before saturation.

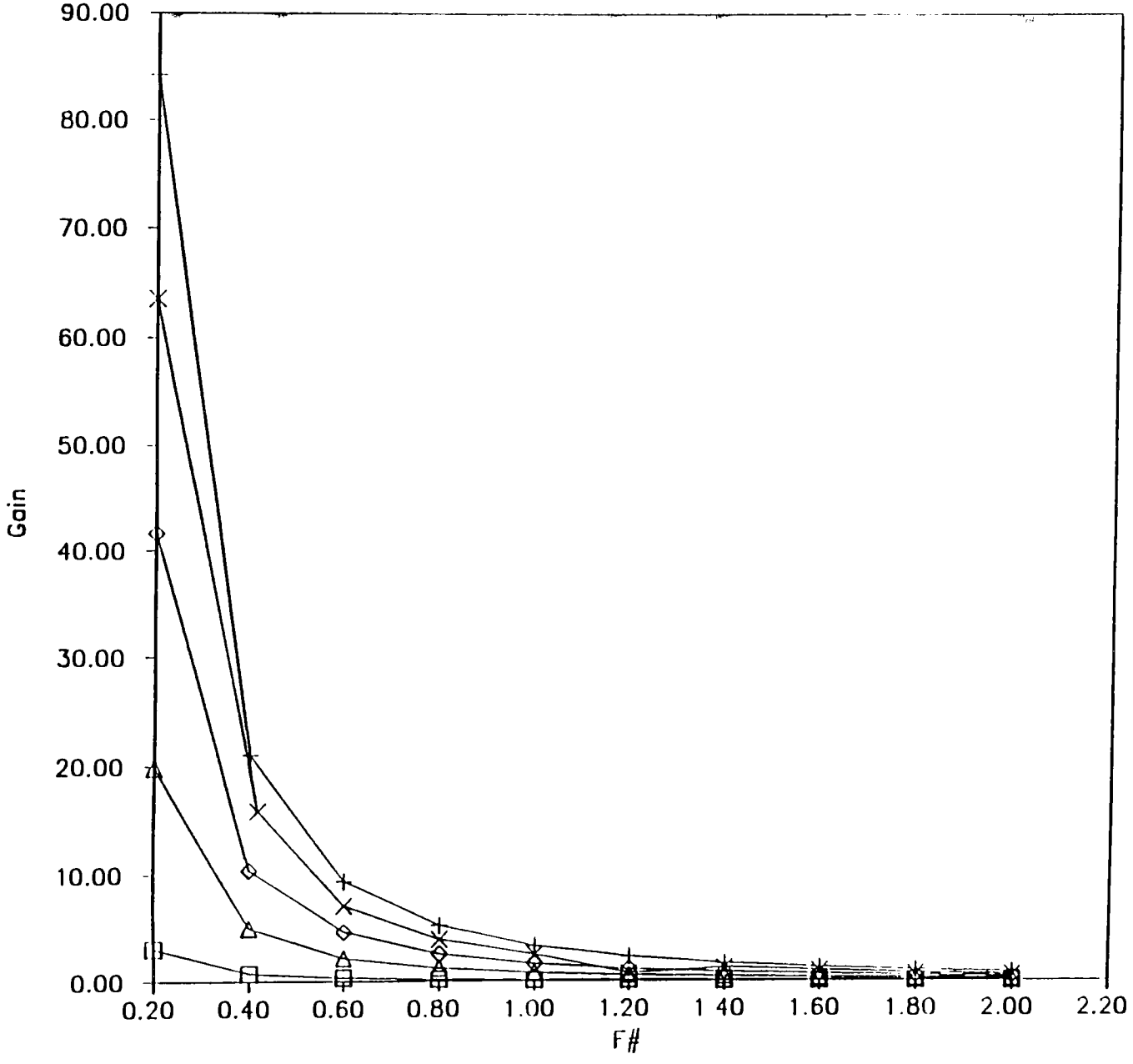

Fig.5 Mean gain is inversely proprtional to the square of the F# of the lens, and inversely proportional to M, where M is the size of the CCD divided by the size of the screen.

Fig.5.1 Gain vs. F# (M = 0.1)

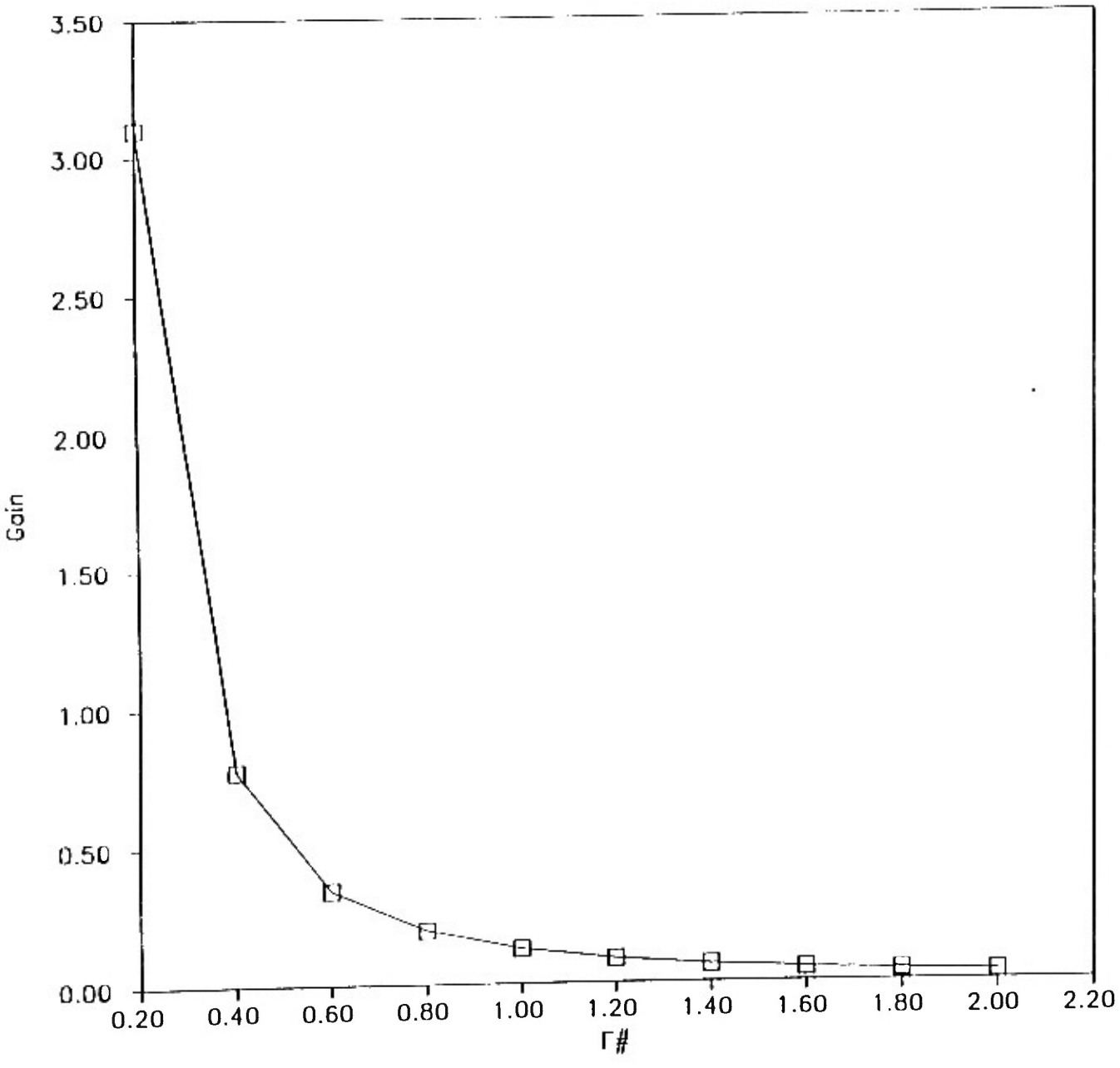

Fig.5.2 Gain vs. F# (M = 0.3)

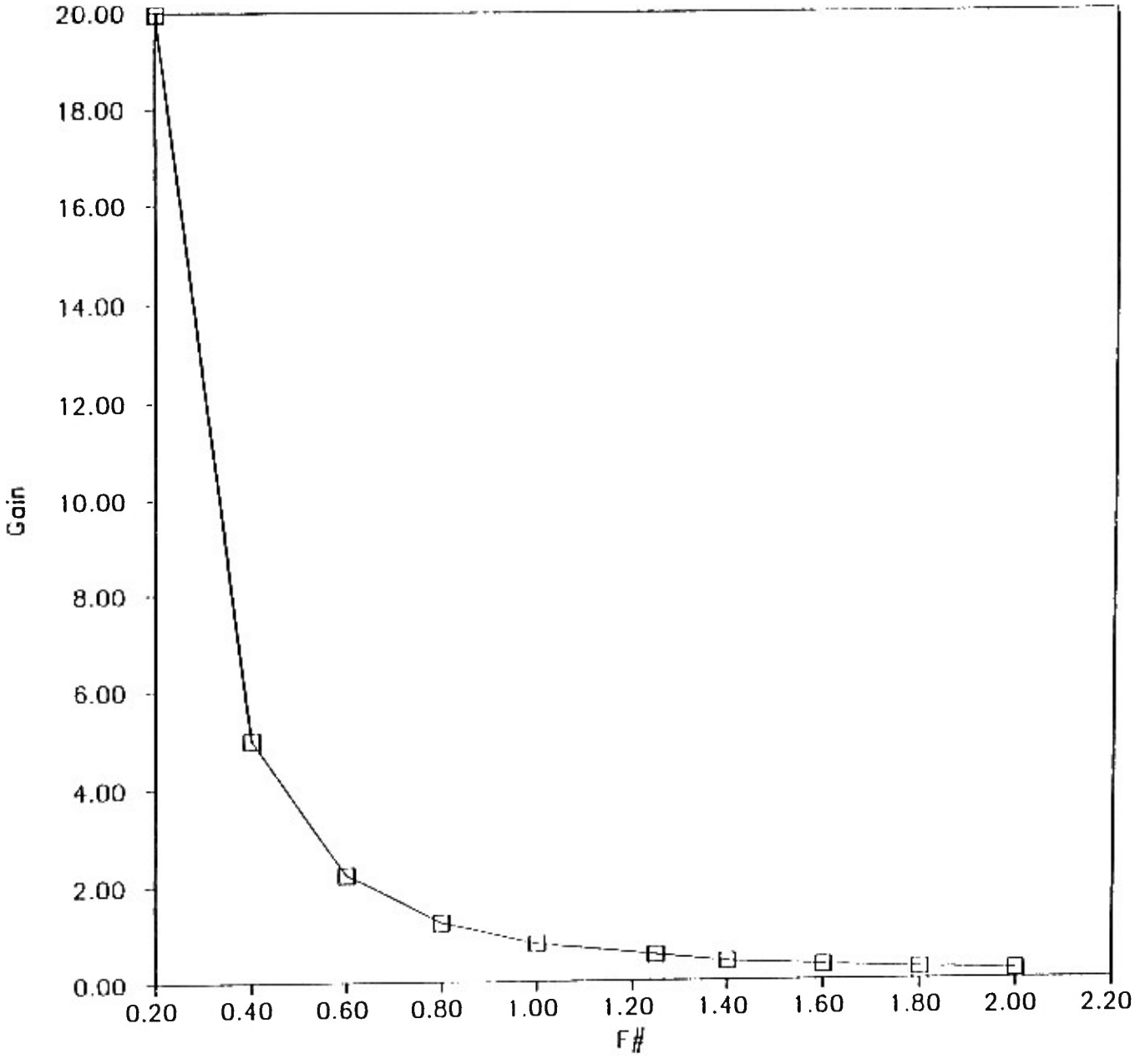

Fig.5.3 Gain vs. F# (M = 0.5)

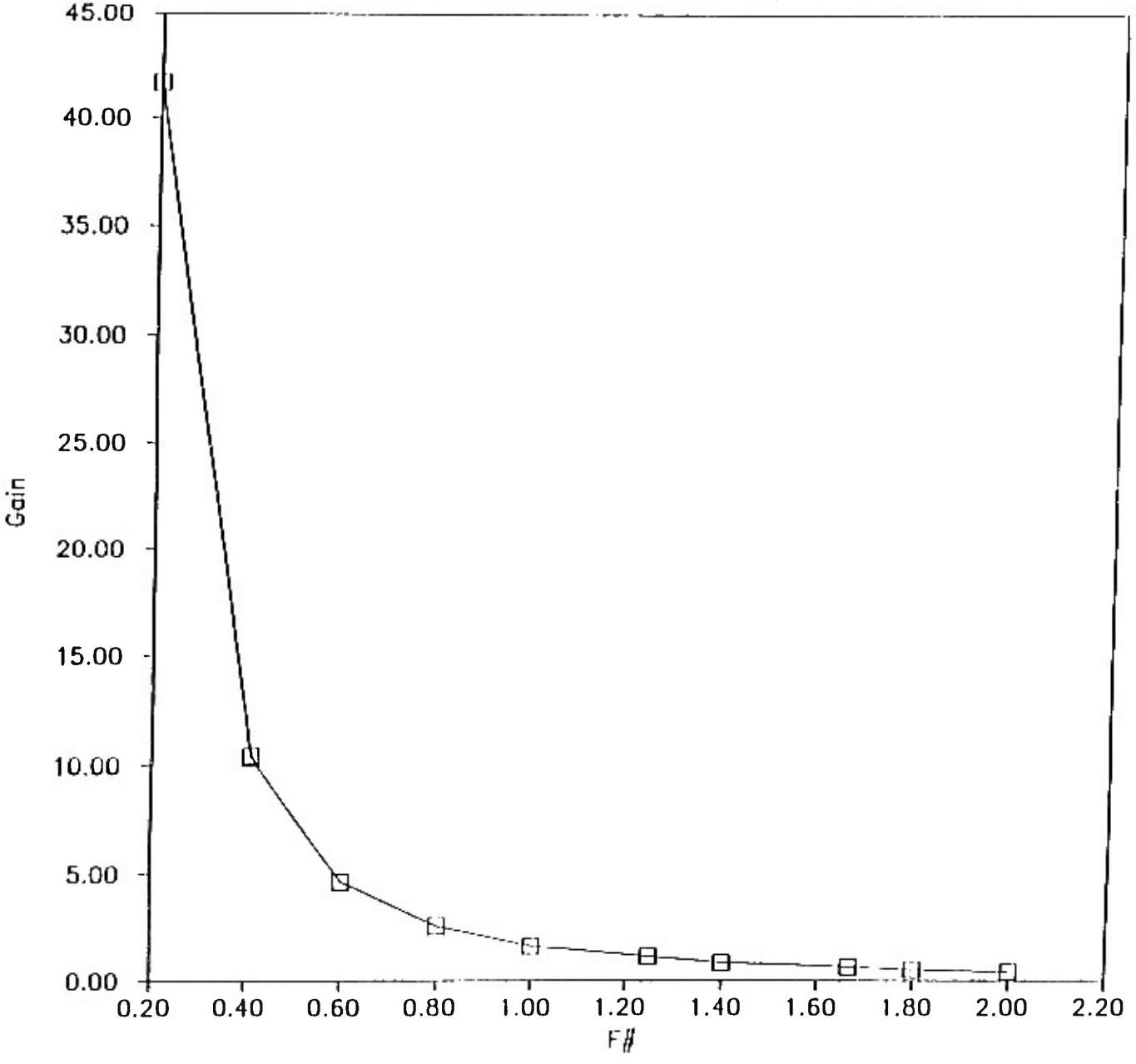

Fig.5.4 Gain vs. F# (M = 0.7)

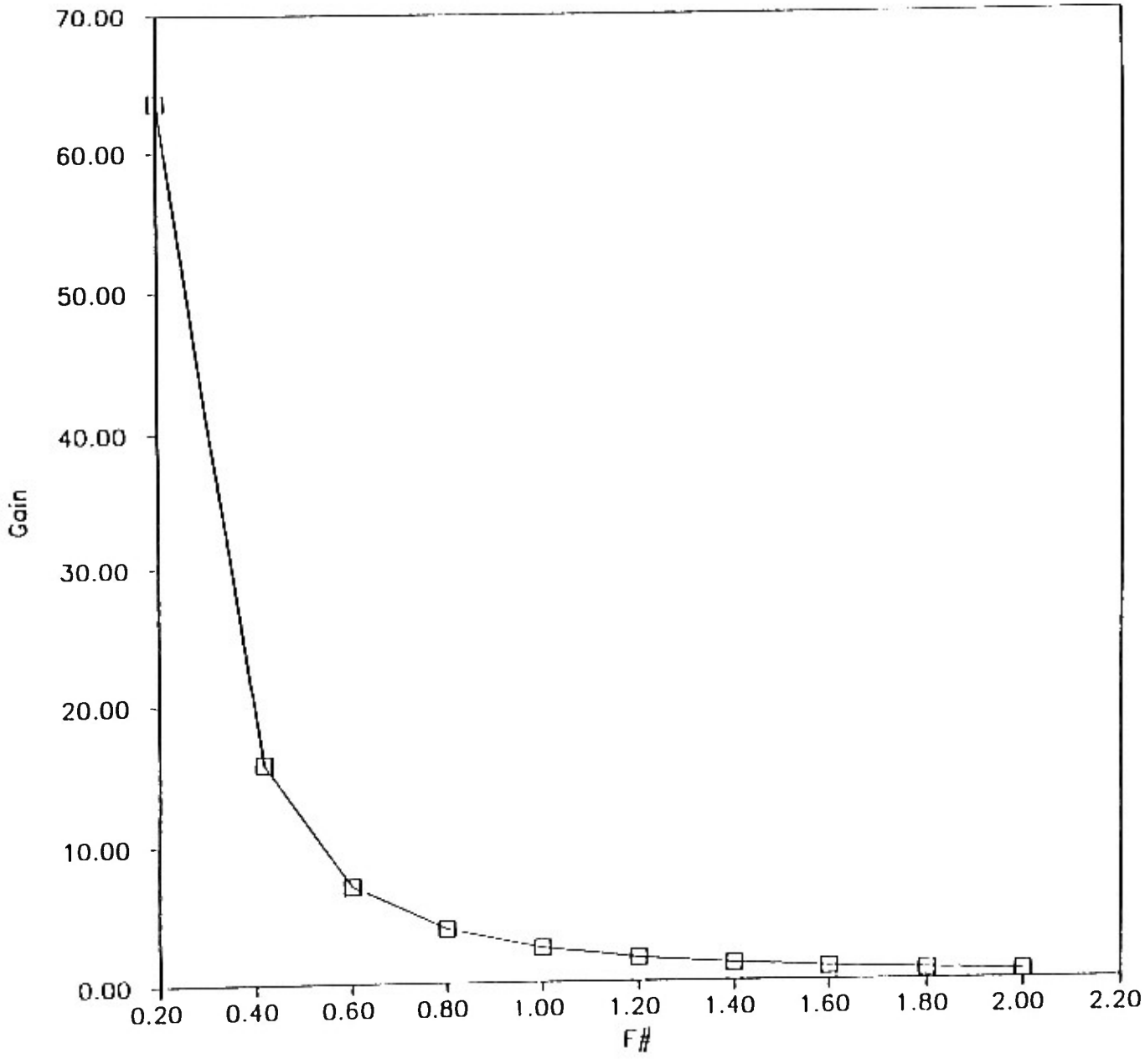

Fig.5.5 Gain vs. F# (M = 0.9)

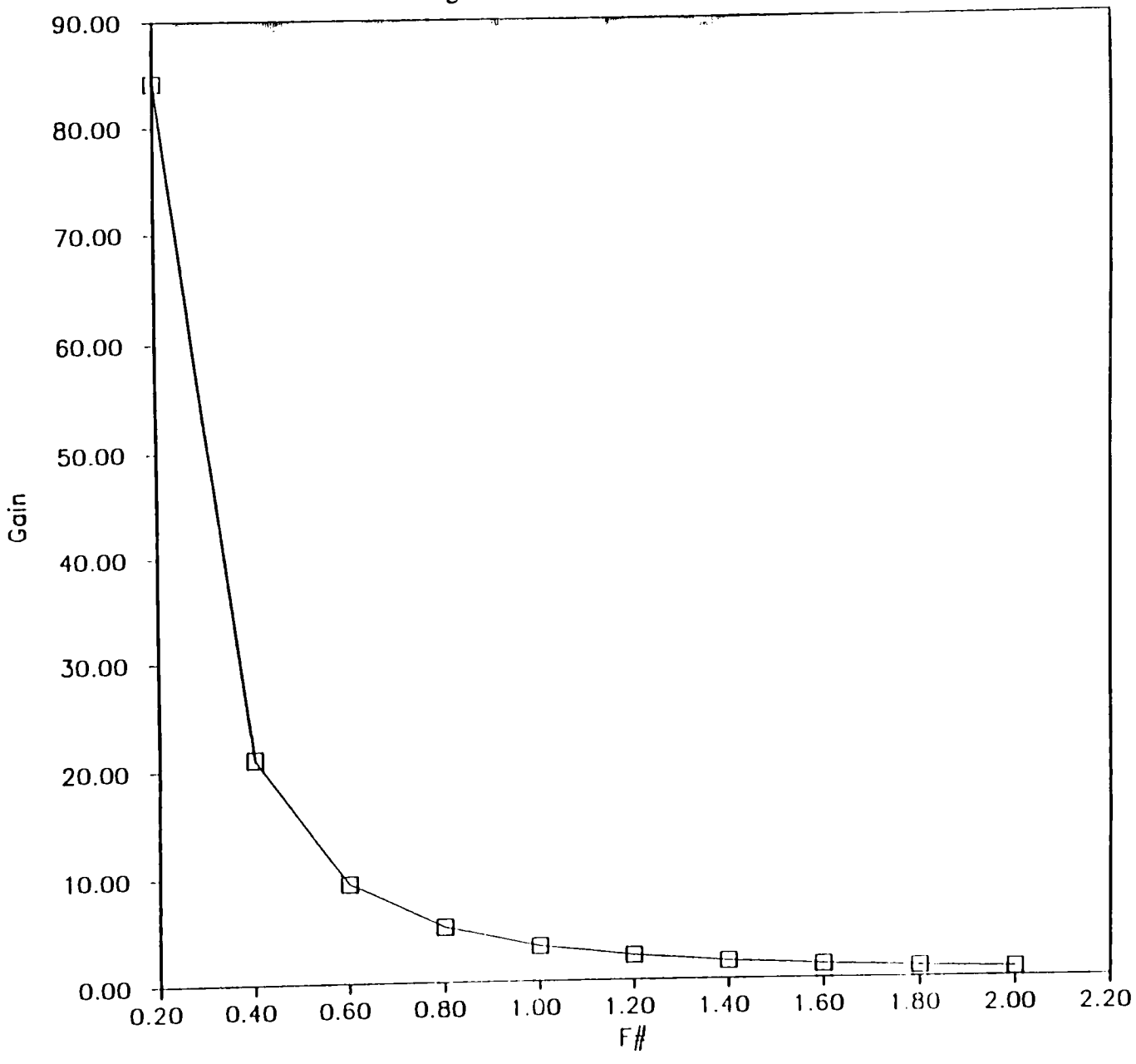

Fig.6 MTF of the lens

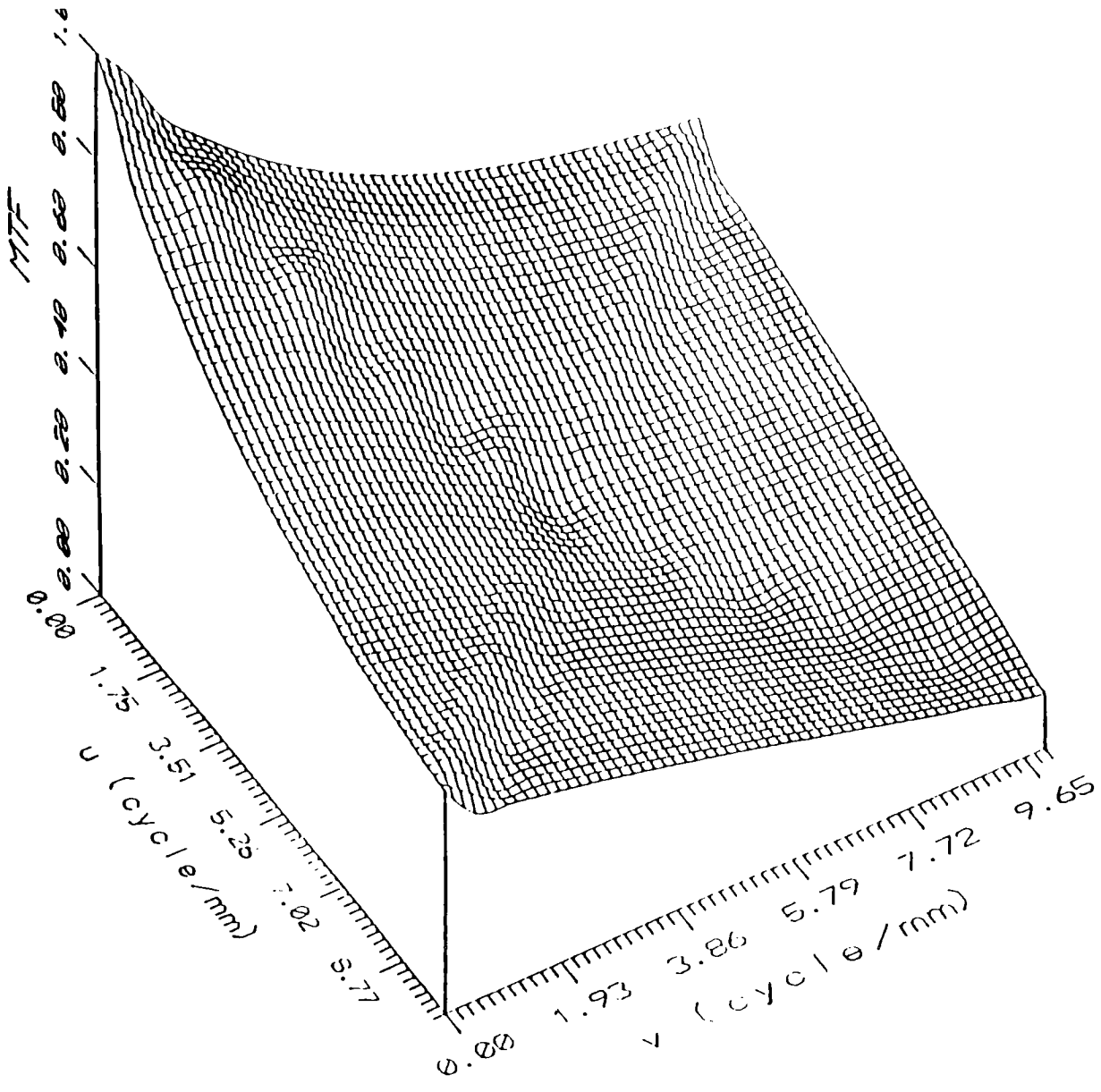

Fig.7 MTF of the screen

Fig.8 MTF of the CCD

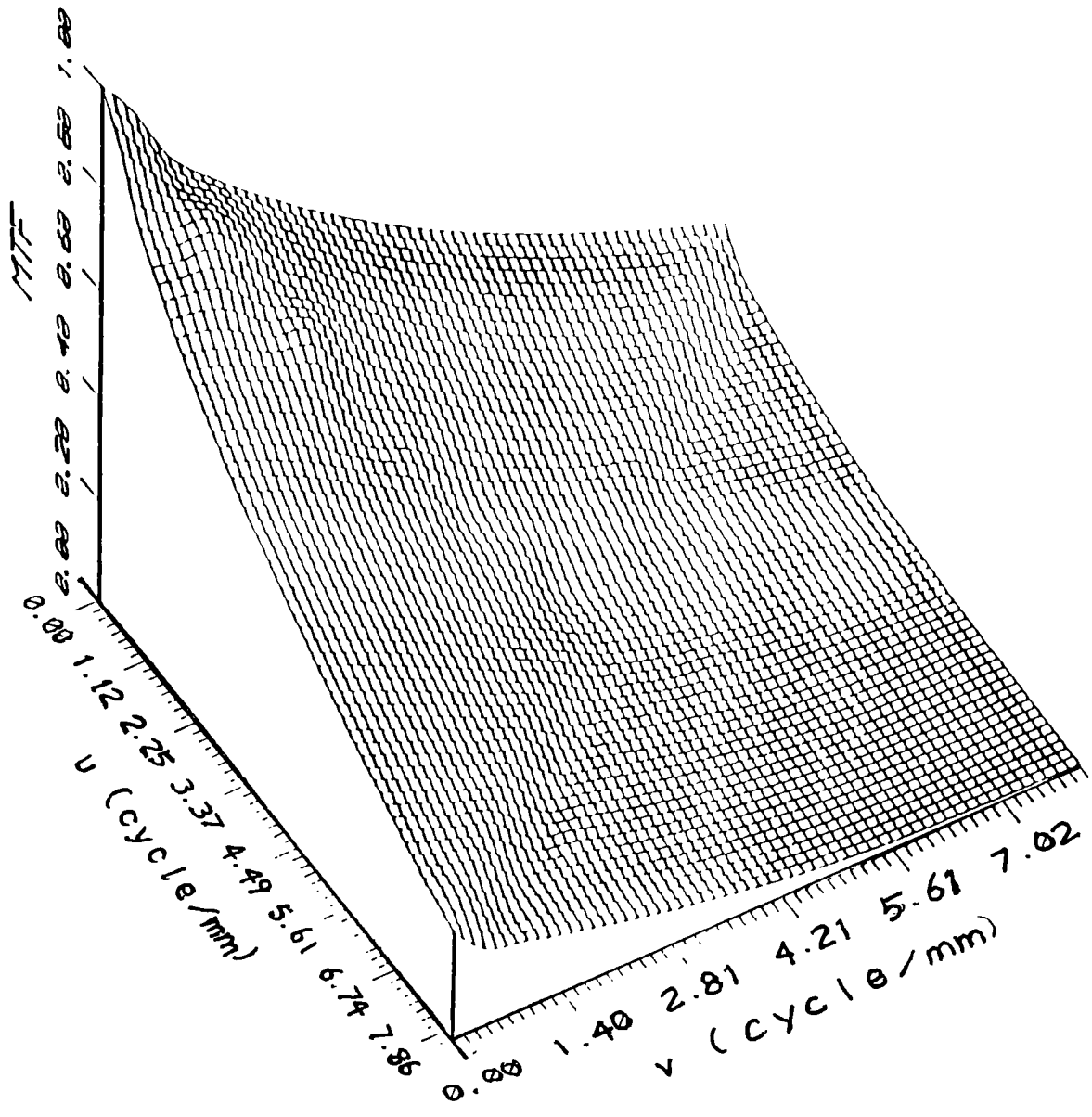

Fig.9 The MTF of the system is a product of the MTFs of the screen, lens and CCD.

Fig.10 Wiener Spectrum of the system

Fig.11 DQE of the system

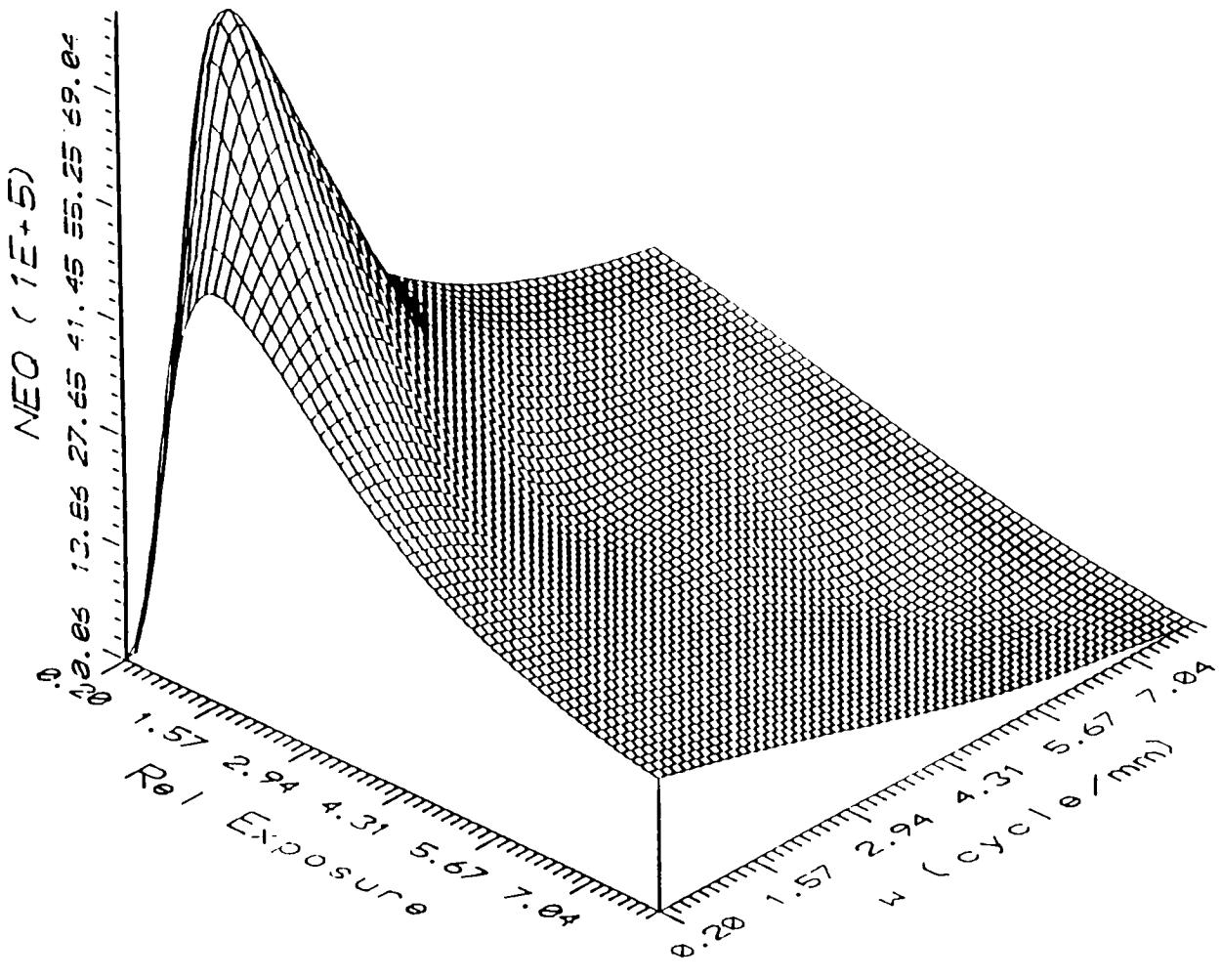

Fig.12 NEQ of the system

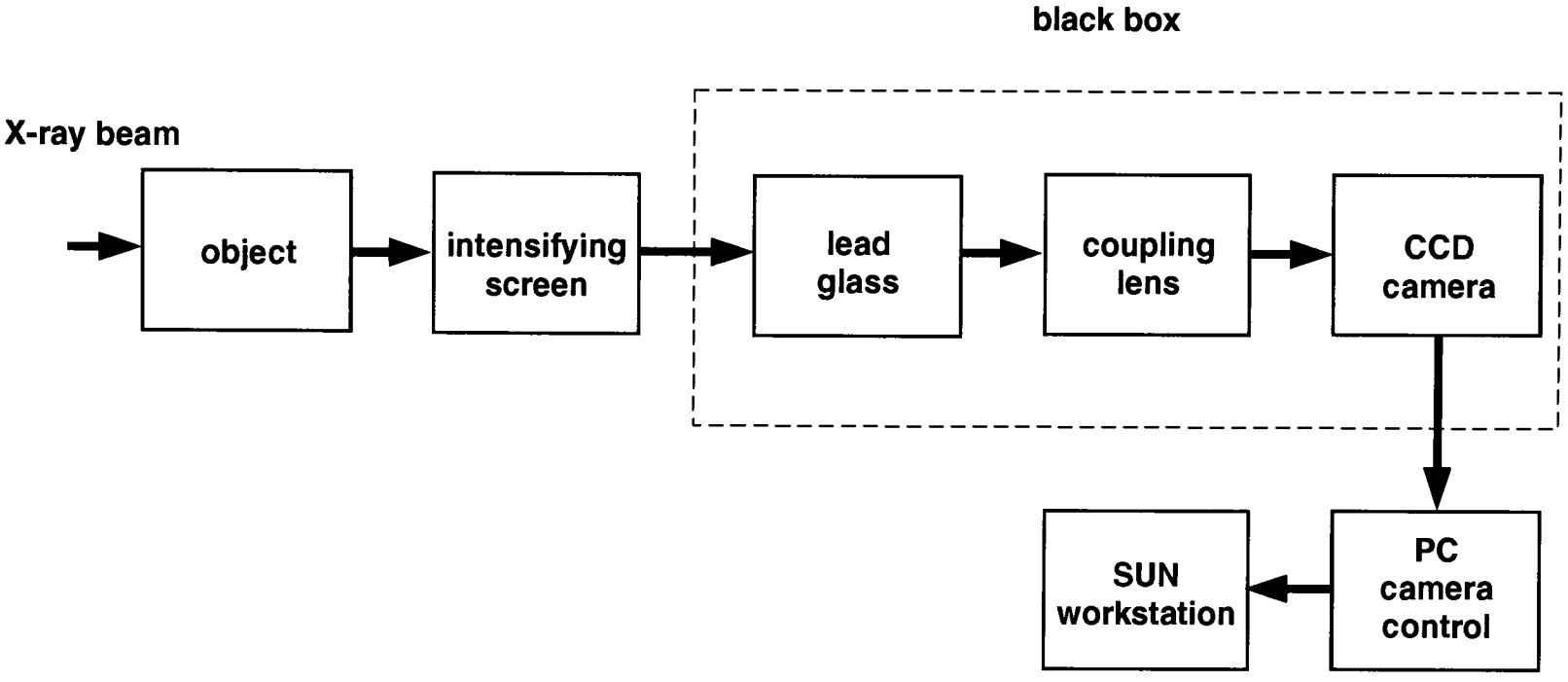

Fig.13 The system set-up for evaluation.

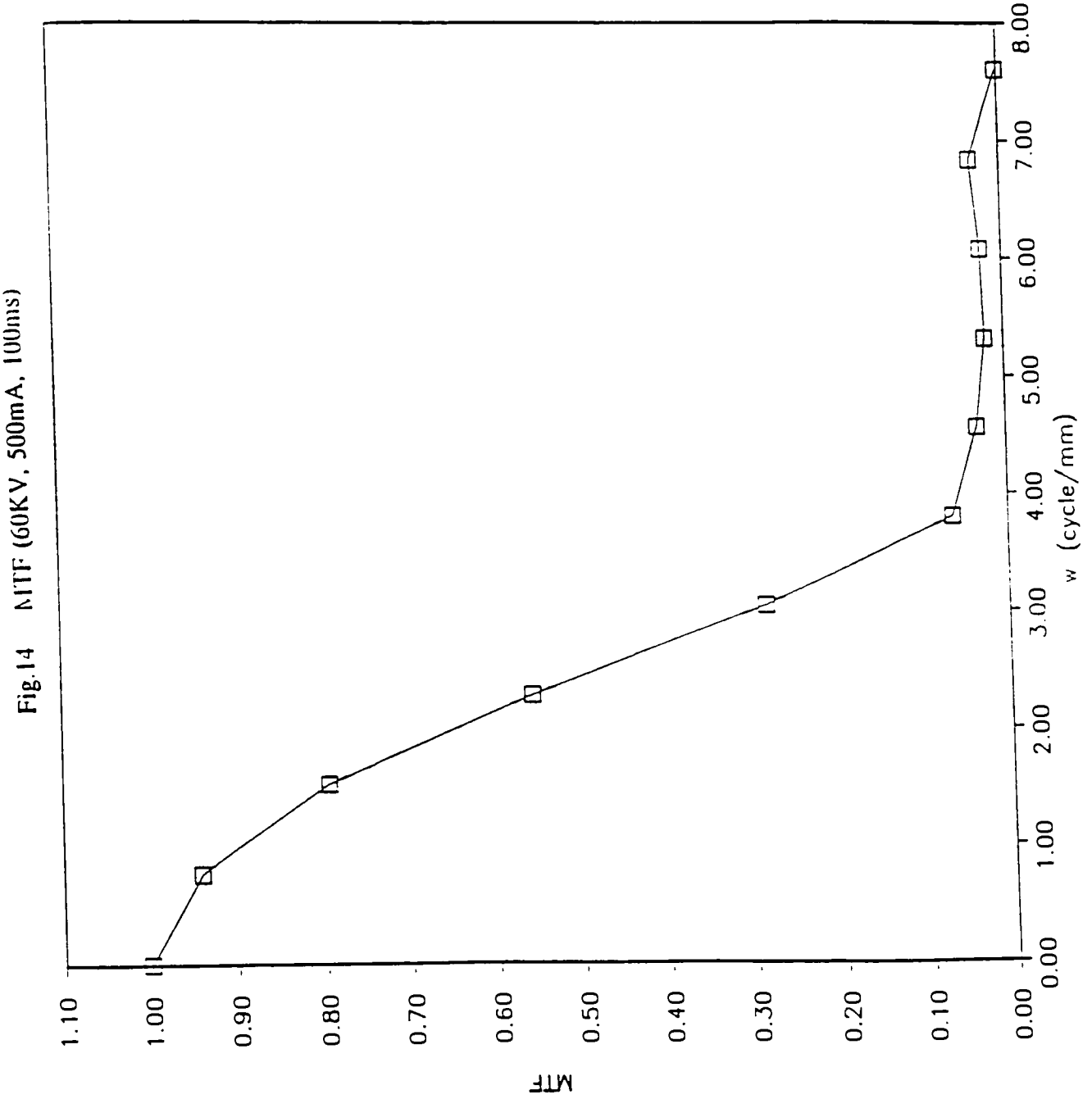

Fig.14 MTF (60KV, 500mA, 100ms)

Fig.15 MTF (60KV, 500mA, 200ms)

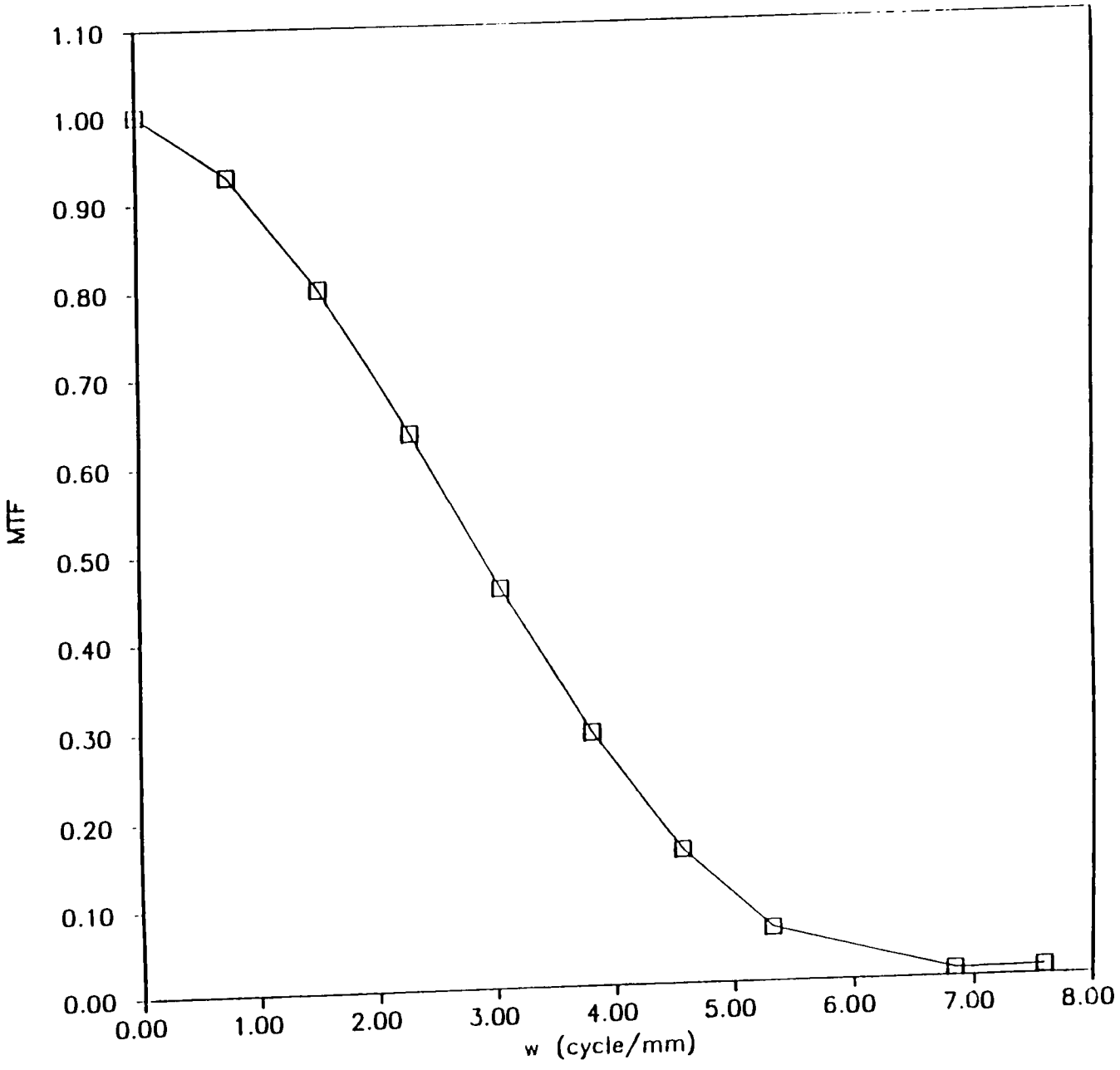

Fig.16 MTF (25KV, 500mA, 2s)

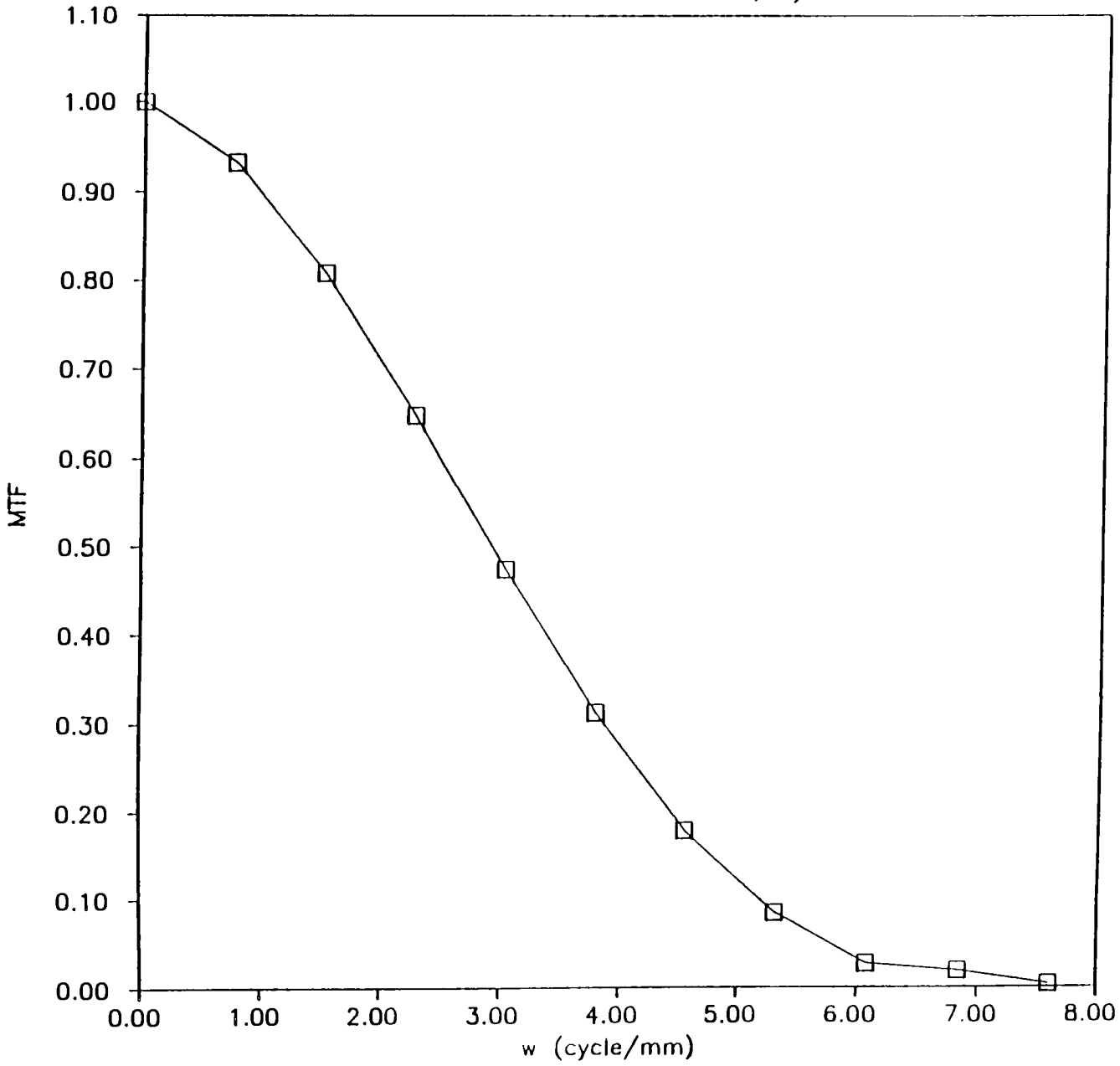

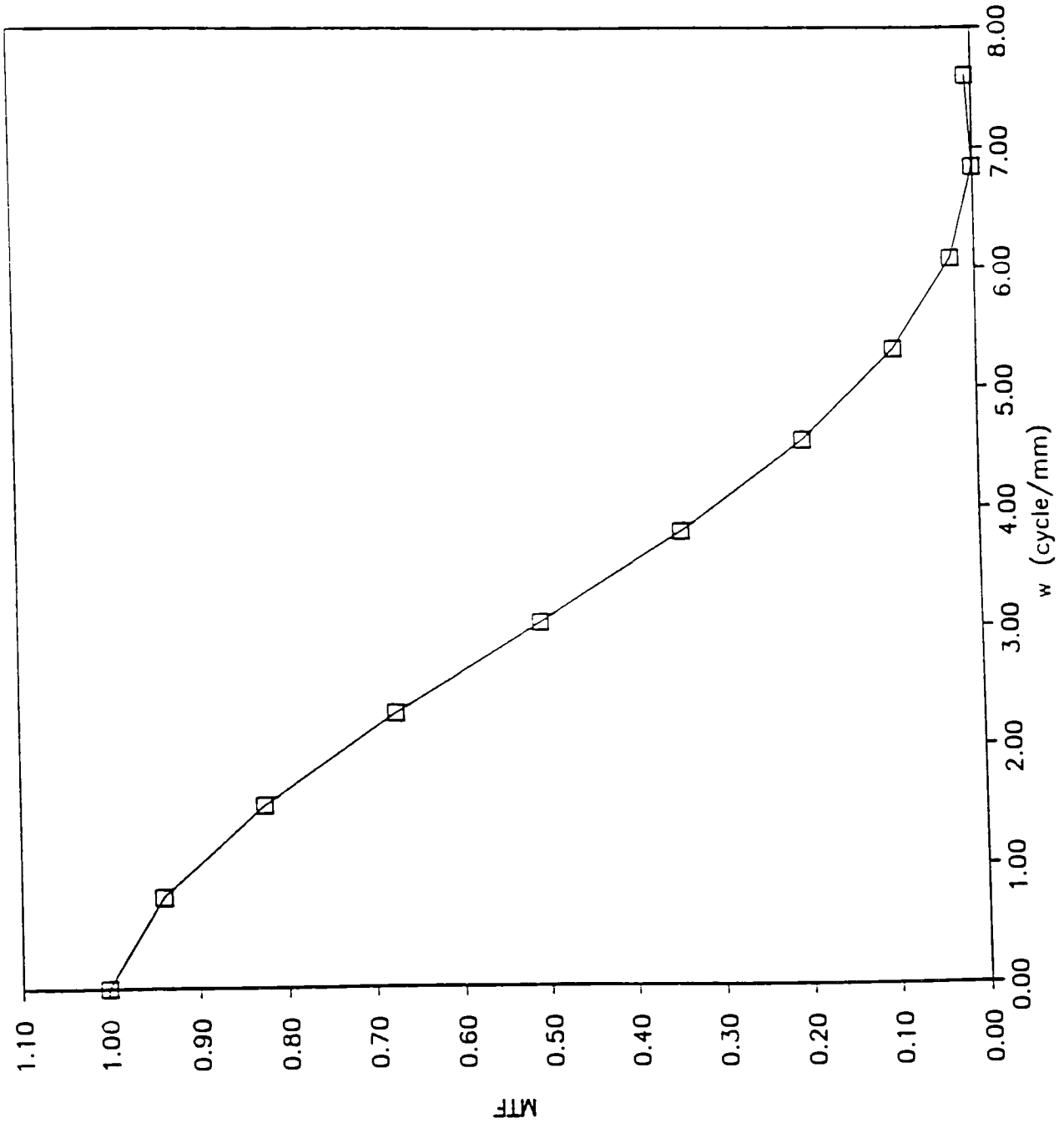

Fig.17 MTF (25KV, 500mA, 100ms)

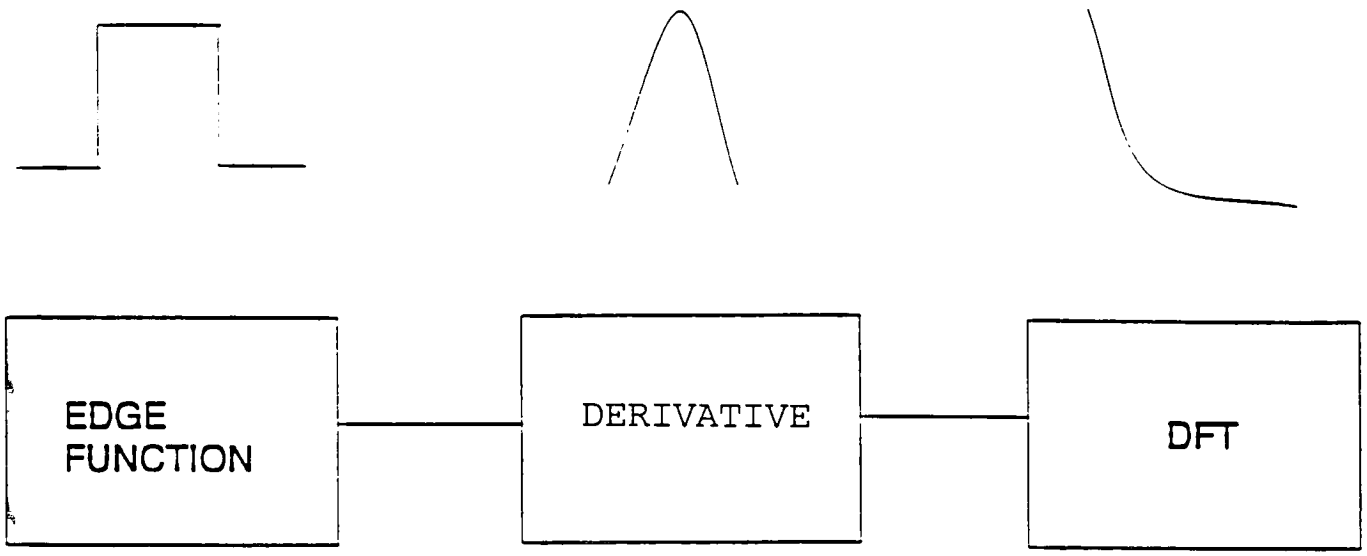

Fig.18 The MTF value for the system was obtained by measuring the edge function, taking it's derivative, and performing the DFT.

Fig.19 The contrast details of the arterial phantom were determined from the ratio of the value at the arterial lines to the background signal.

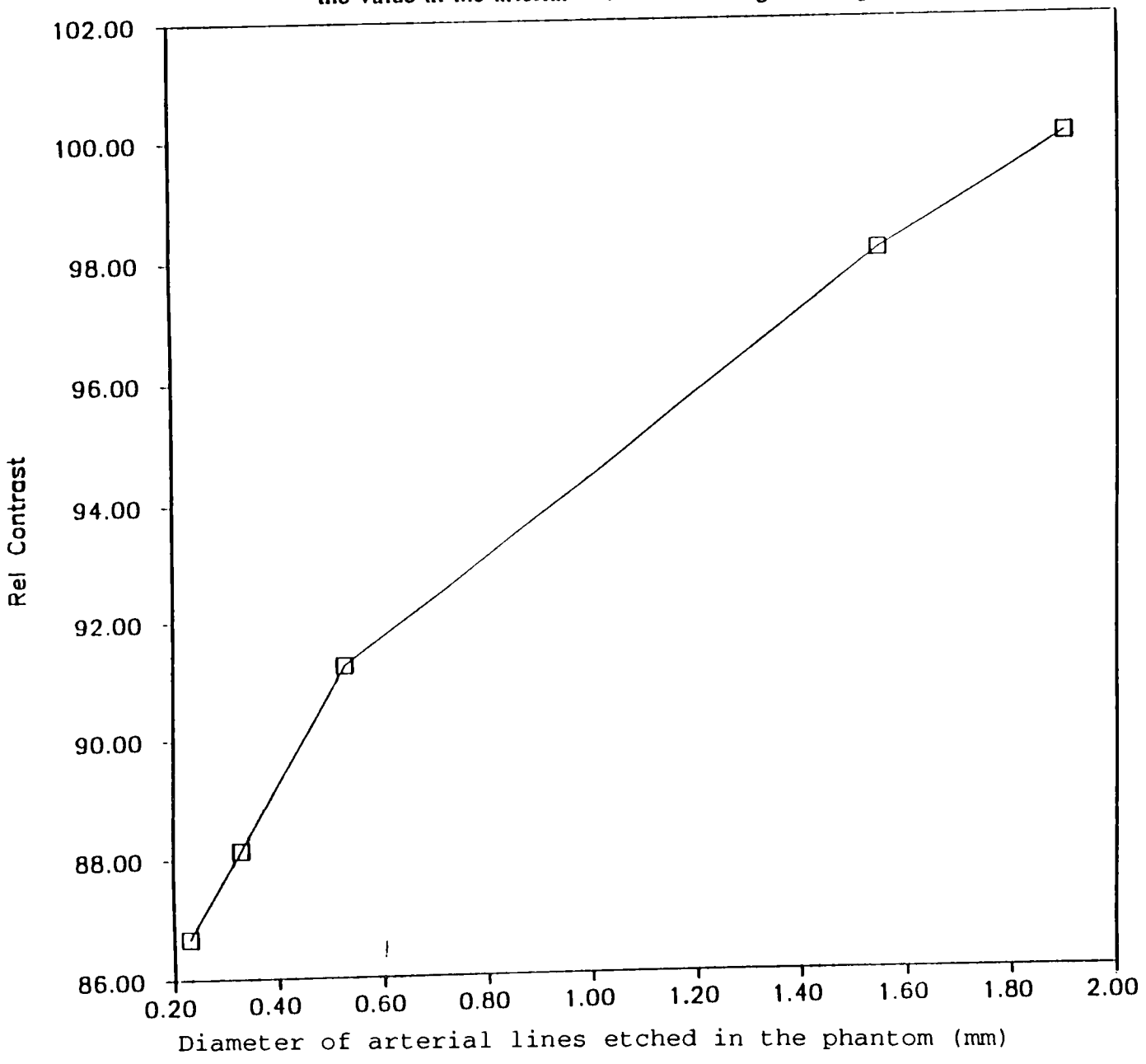

Fig.20 SNR (60KV, 500mA, 100ms)

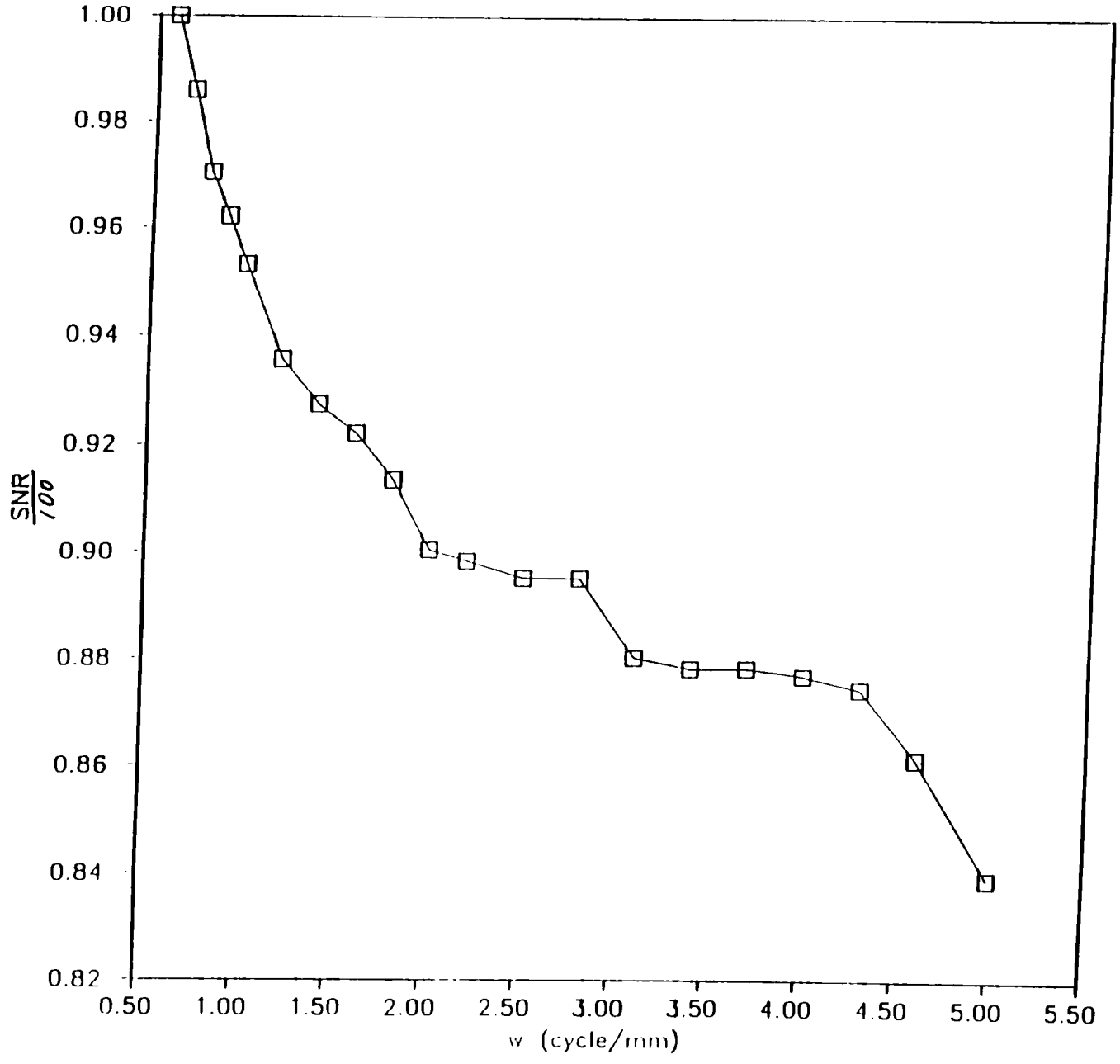

Fig.20 The average signals and average noises were measured at different resolutions.

Fig.21 SNR vs. exposure time

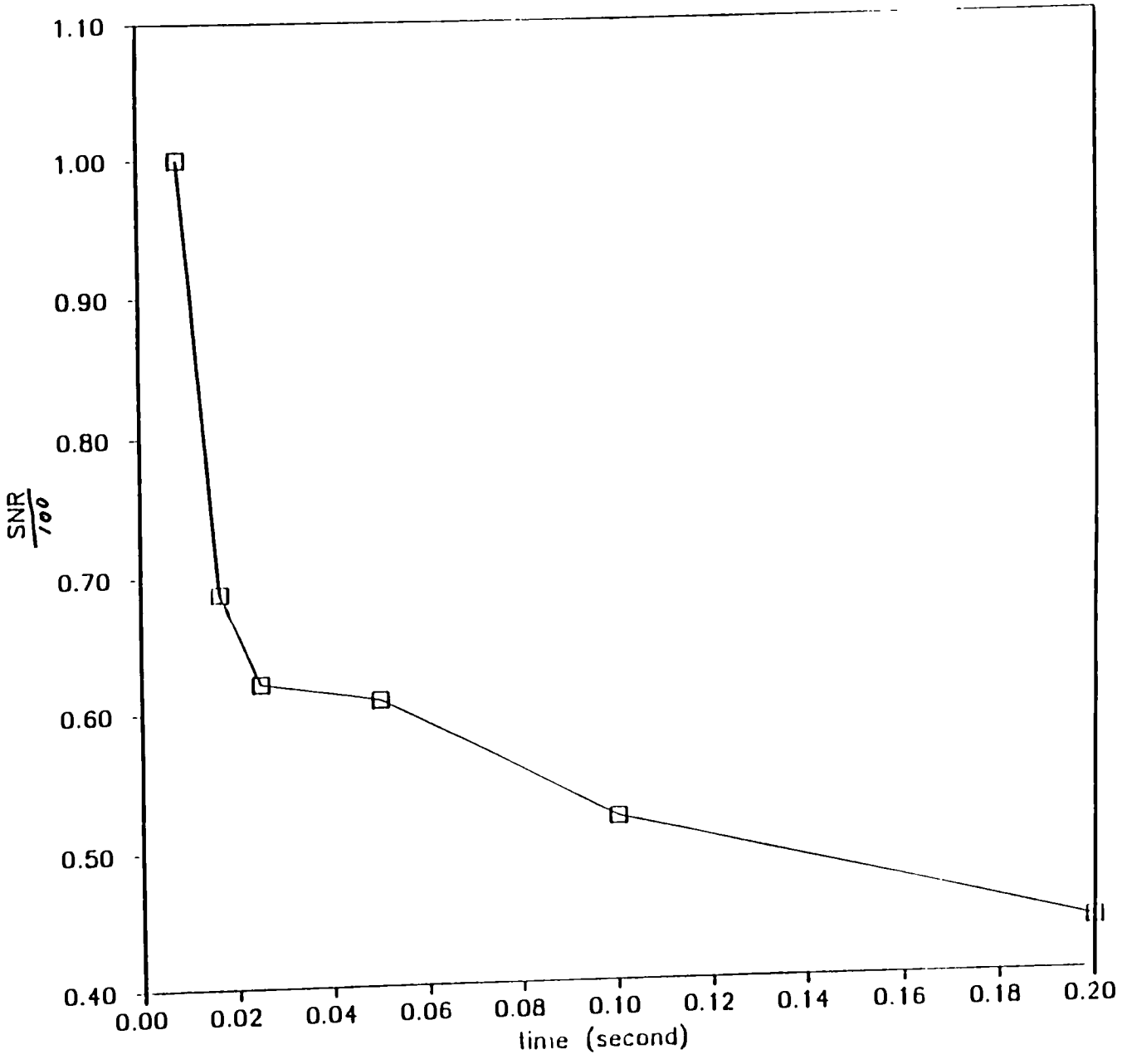

Fig.21 The signal Noise Ratio of the tri-bar image taken at 60KV, 500mA with varying exposure time.

Fig.22 SNR vs. exposure time

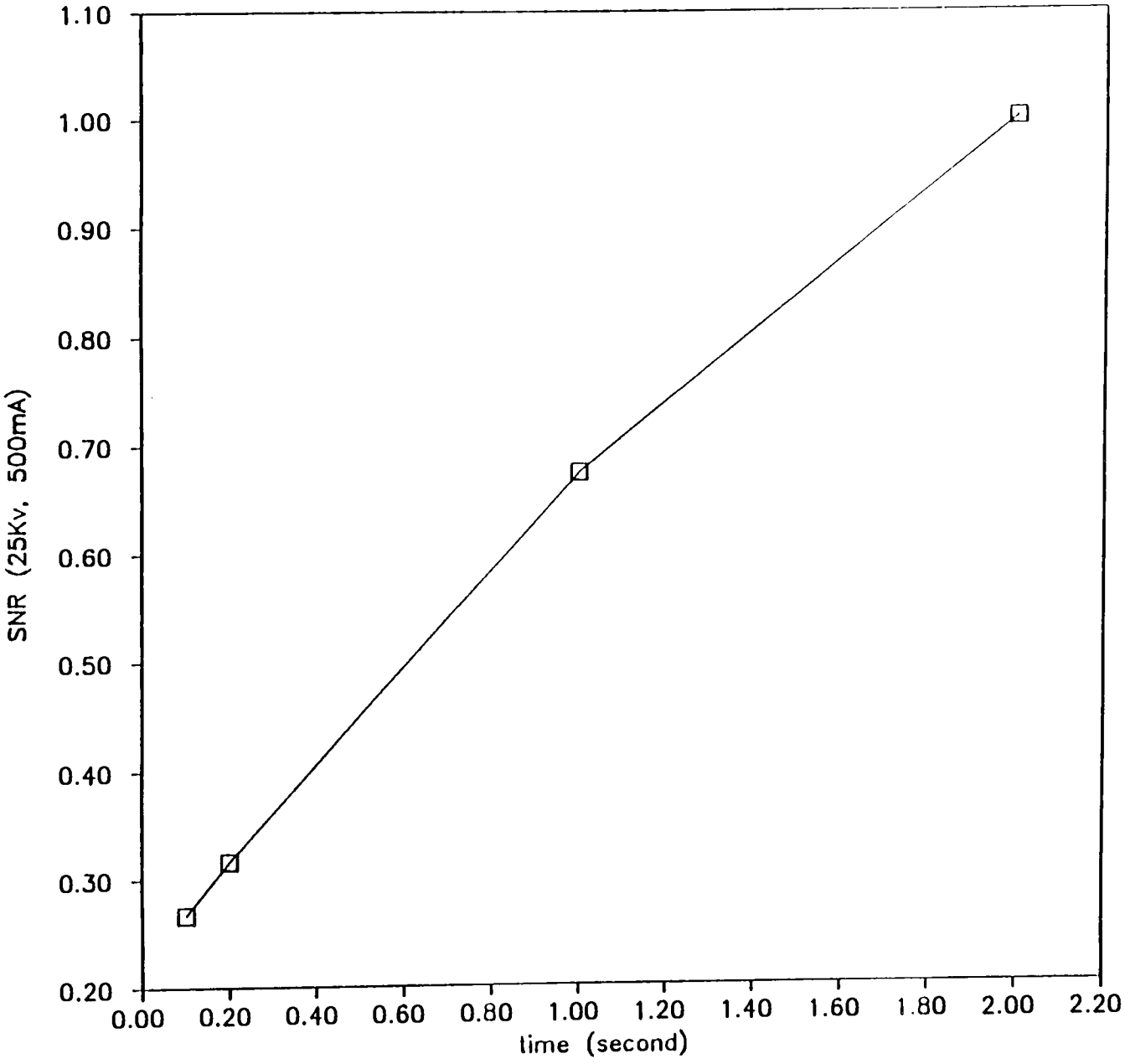

Fig.22 Comparing this with the data in Fig.21 reveals the relationship between the SNR and the exposure time at different energies.

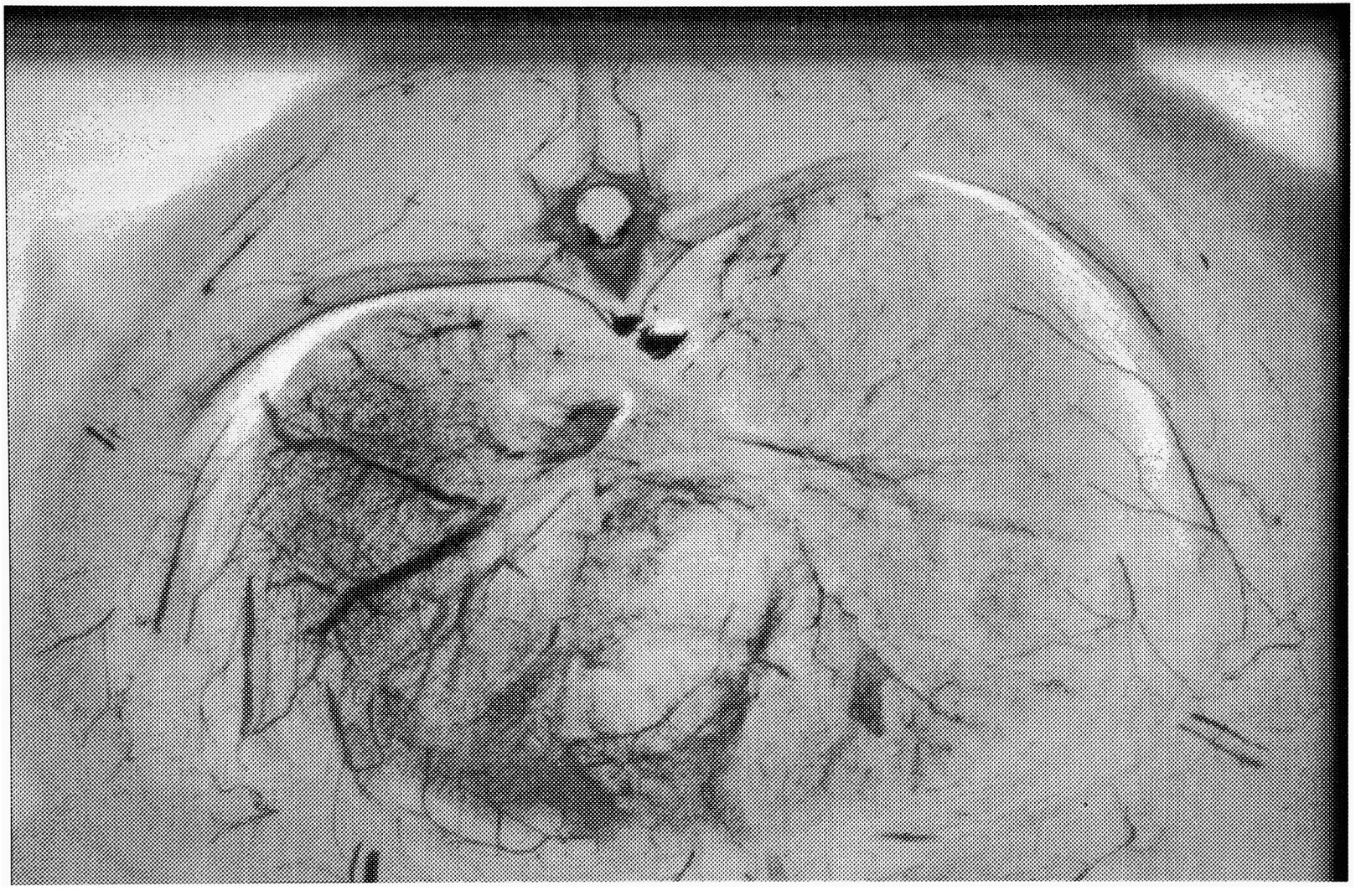

Fig.23 An image of a rabbit liver section taken at 25KV, 500mA, and 500ms.

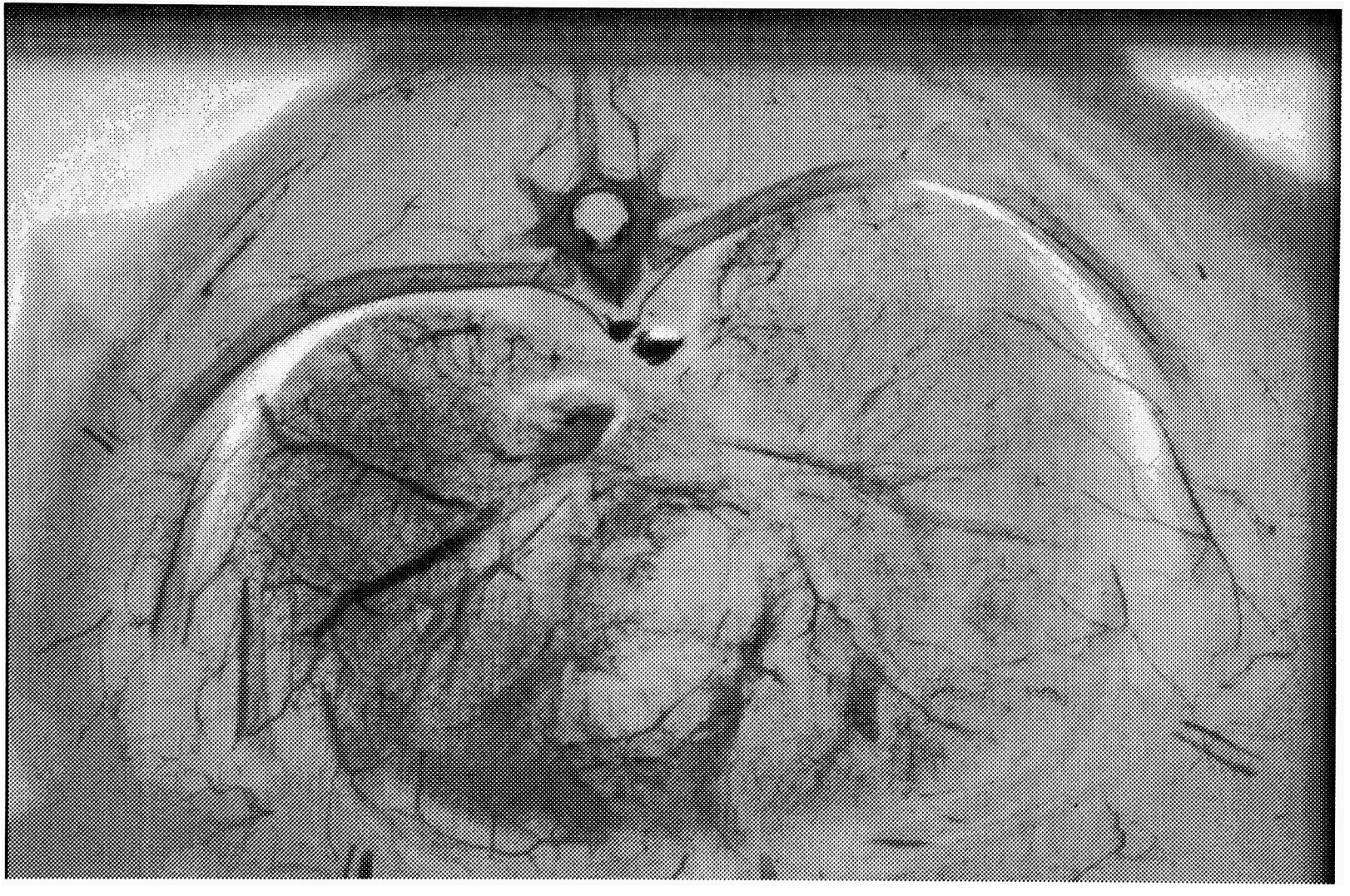

Fig.24 An image of a rabbit liver section taken at 50KV, 500mA, and 500ms.

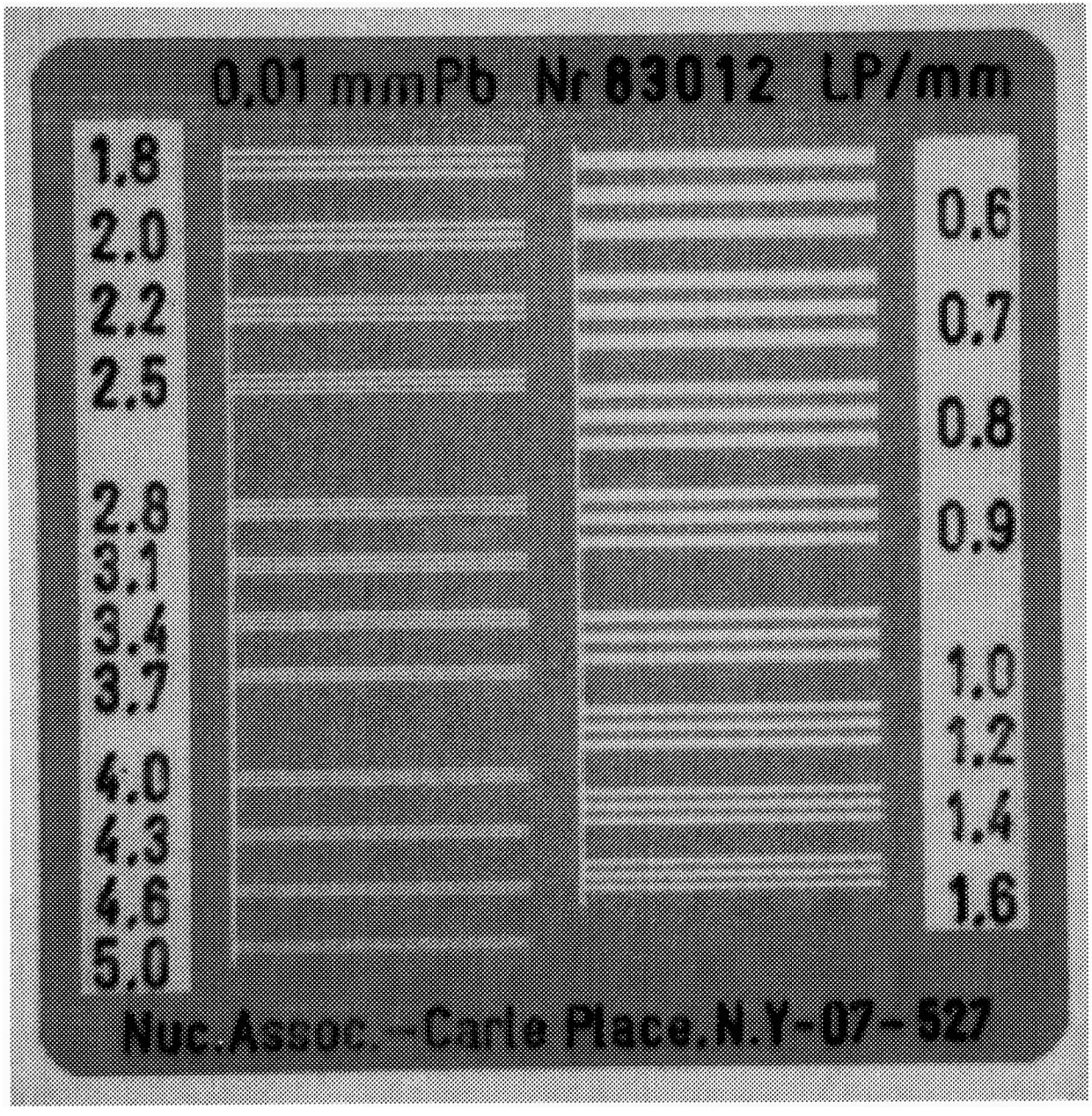

Fig.25 An image of tri-bar tile, taken at 60KV, 500mA, and 100ms.

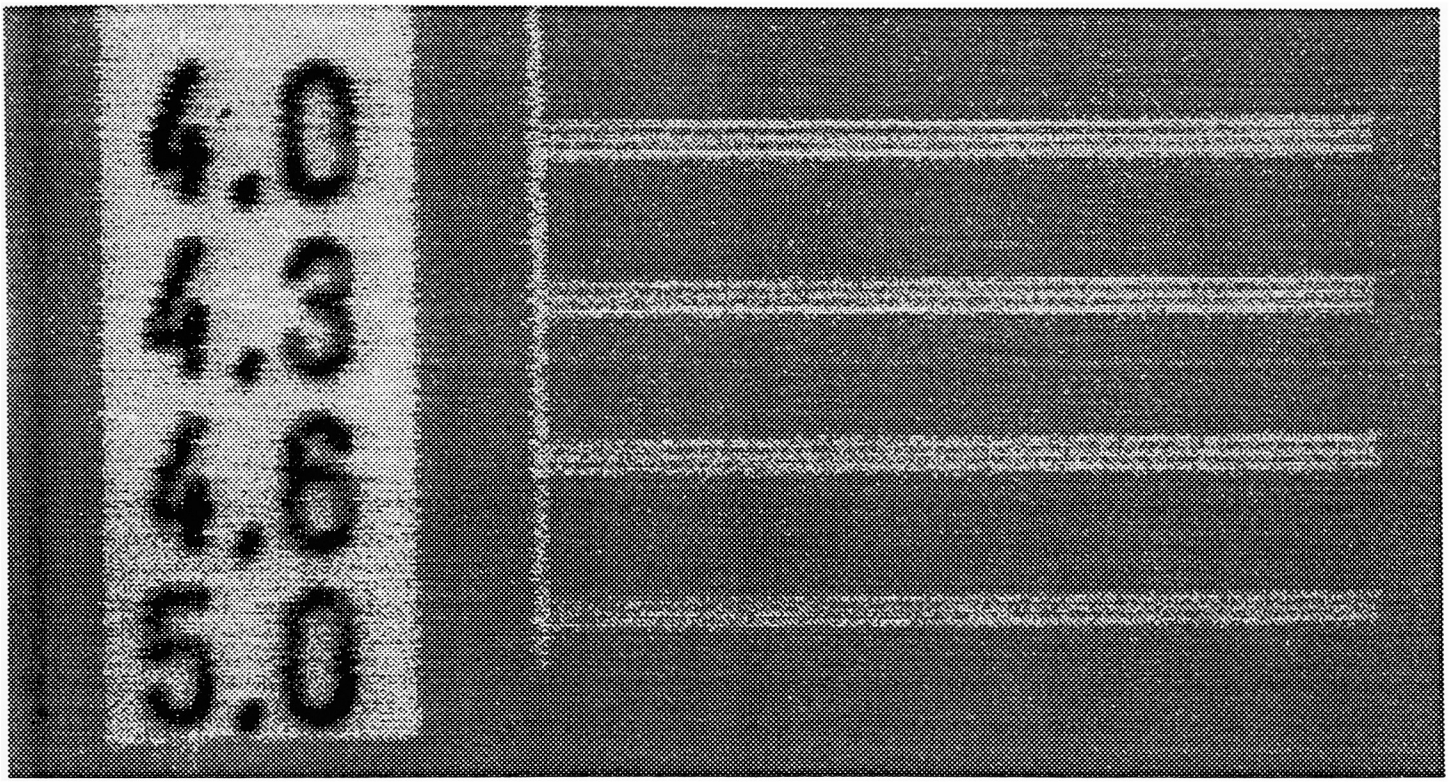

Fig. 25' A close up look of the finest part of Fig. 25

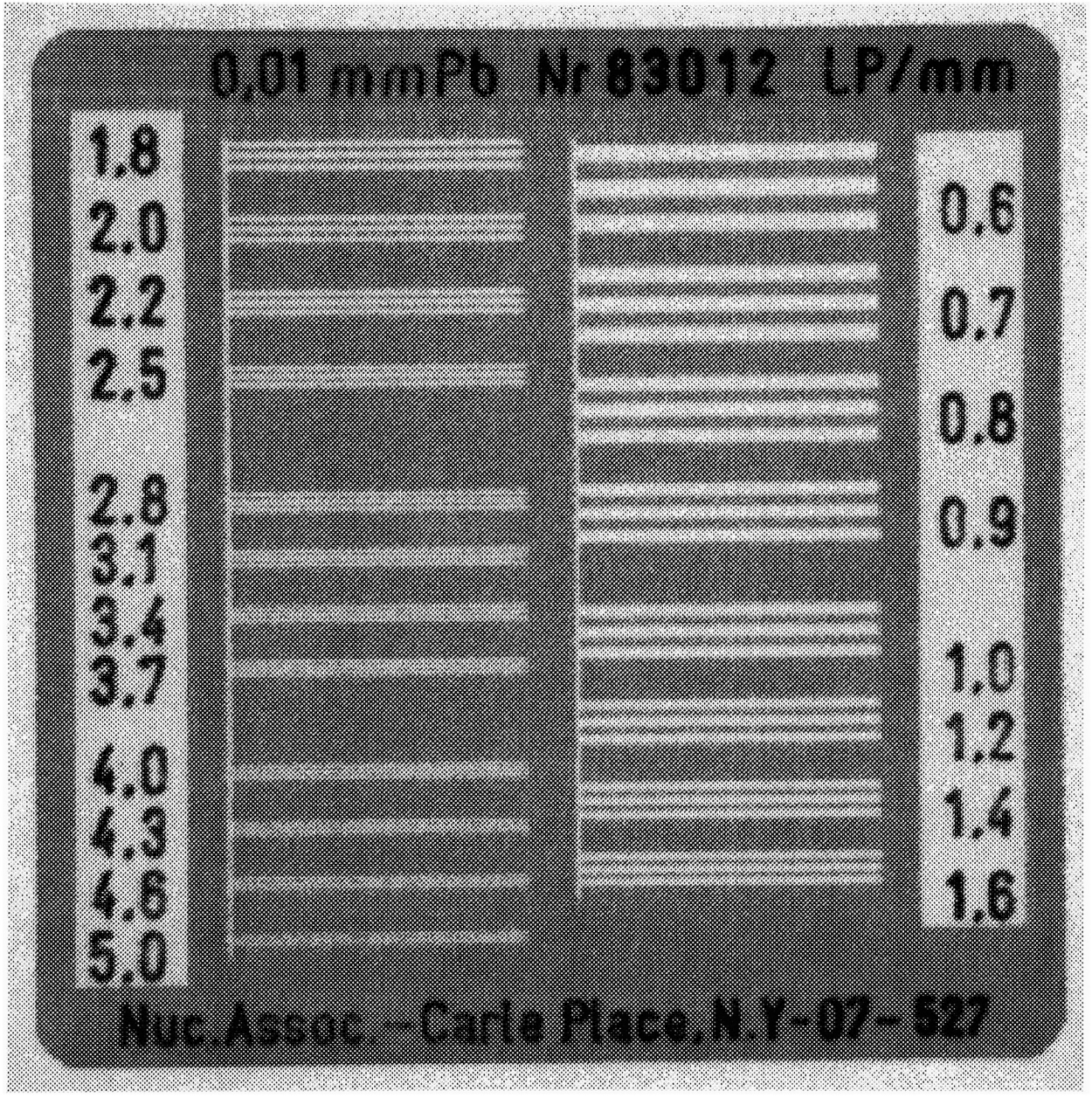

Fig.26 An image of tri-bar tile, taken at 25KV, 500mA, and 100ms.

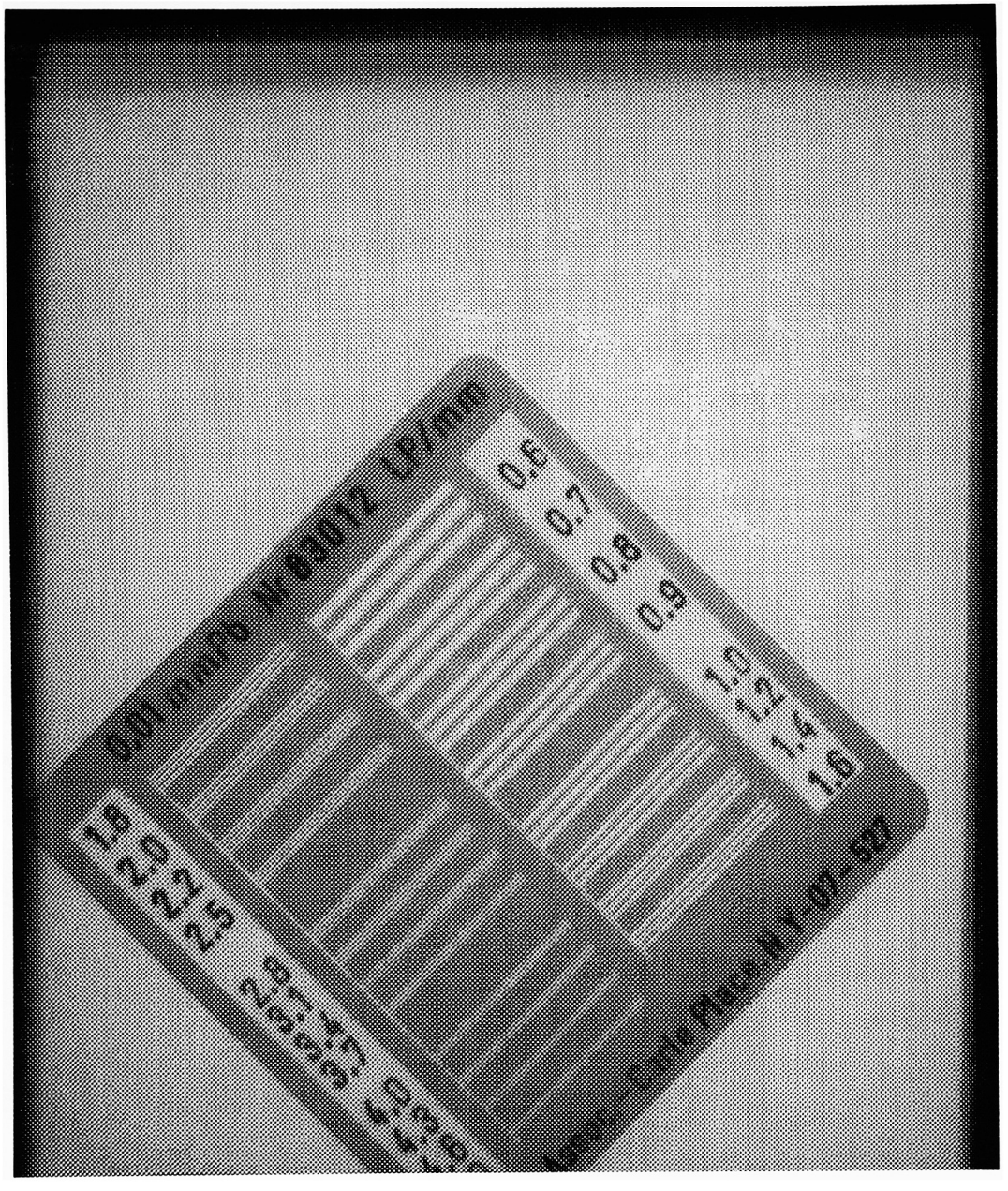

Fig.27 An image of tri-bar tile attached to a 1 inch thick piece of lucite, taken at 25KV, 500mA, and 100ms.

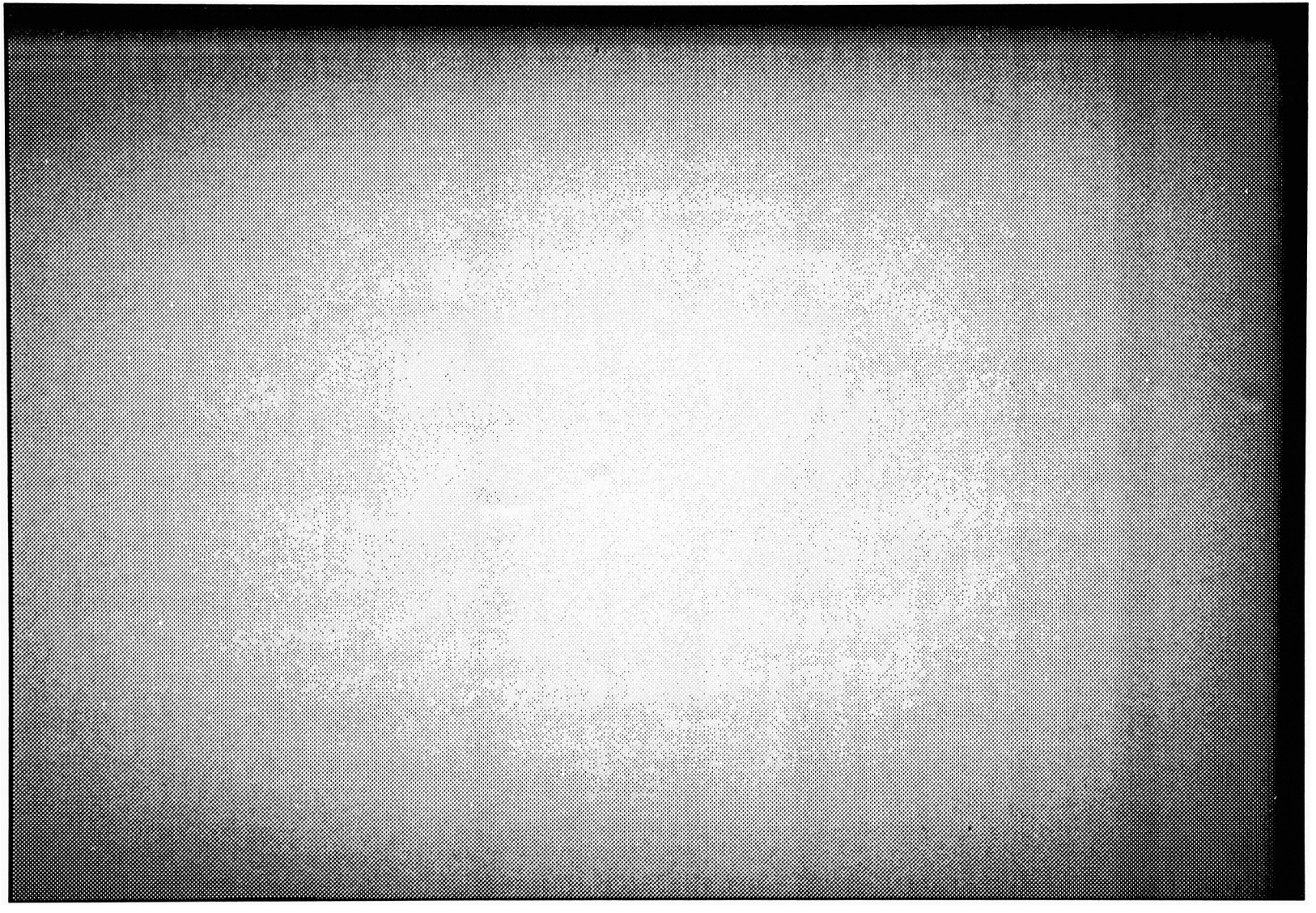

Fig.28 An image of arteries etched in a 1 inch thick piece of lucite. It was taken at 25KV, 500mA, and 2sec.

NAME	VOL (KV)	MA	SEC	CONTRAST (MAX/MIN)	RESOLUTION
UR1	60	500	1/20	215/51	5+
UR3	60	500	1/40	198/51	5-
UR4	60	500	1/60	196/51	4.6
UR5	60	500	1/120	195/51	4.0
UR6	60	500	1/10	269/51	5+
UR7	60	500	1/5	401/51	5+
UR12	25	500	1/5	193/52	5-
UR13	25	500	1	308/51	5
UR14	25	500	2	558/52	5
UR15	25	500	1/10	189/51	4.6
URP1	25	500	1	825/51	5
URP2	25	500	2	1630/51	5
URP3	25	500	1/5	323/51	5

Table.1 Contrast of each image was measured by reading the maximum and minimum gray values.

Image	Voltage (KV)	Current (mA)	Time (SEC)	Signal	Noise
URP1	25	500	1	146	3
URP2	25	500	2	234	4.5
URP3	25	500	0.5	86.3	1

Table.2 Signal and noise values from images of a phantom block taken at 25KV and 500mA at 0.2sec.. 1sec.. 2sec.

IMAGE	NPIX	MEAN	STDDEV	MIN	MAX
UR1	4145287	69.35	23.43	51	215
UR 3		62.76	11.66	51	198
UR4		60.31	7.743	51	196
UR5	SAME	50.24	3.87	51	195
UR6		83	46.66	51	269
UR7		110.1	93.66	51	401
UR12		64.38	15.04	52	193
UR13		99.58	76.42	51	308
UR14	SAME	143.4	153.3	52	558
UR15		60.06	7.438	51	189
URP1		116.3	135.7	51	825
URP2	SAME	178.8	279	52	1630
URP3		76.54	46.56	51	323

TABLE 3. STATISTICS OF IMAGES

V. REFERENCE

1. W.Kuhl, "X-Ray Imaging", <<ELECTRONIC IMAGING>> 309-325, London, New York: Academic Press (1979)
2. H.Roehrig, S.Nudelman and T.Y.Fu, "Electro-optical devices for use in photoelectronic digital radiology", <<ELECTRONIC IMAGING IN MEDICINE>> 82-125, New York, NY: American Institute of Physics (c1984)
3. S.P.Wang, J. Zeilenga, R.P.Hunt, D.F.Specht, R.S.Enck, "High Resolution Digital Radiography Using a Proximity Type Image Intensifier", SPIE, 454, 250 (1984)
4. H.Roehrig, W.J.Dallas, T.W.Ovitt, R.D.Lamoreaux, R.Vercillo, and K.McNeill, "A high resolution X-ray imaging device", SPIE, 1072, 88 (1989)
5. H.Roehrig, T.W.Ovitt, W.J.Dallas, R.D.Lamoreaux, R.Vercillo, K.M.McNeill, "Development of a high resolution X-ray imaging device for use in coronary angiography", SPIE, 767, 144 (1987)
6. R.Shaw and R.L.VanMetter, "An analysis of the fundamental limitations of screen-film systems for X-ray detection", SPIE, 454, 133 (1984)
7. E.Caruthers, "Monte Carlo studies of image spread by X-ray intensifying screens", SPIE, 535, 140 (1985)
8. R.VanMetter, "Spectrum of Kodak Min R", private communication (1990)
9. R.K.Swank, Journal of Applied Physics 44. 4199 (1973)
10. P.D.Burns, "Signal-To-Noise Ratio Analysis Of Charge-Coupled Device

Imagers", SPIE, 242, 187 (1990)

11. P.D.Burns, "Image Signal Modulation and Noise Characteristics of Charge-Coupled Device Imagers," SPIE, 1071, 141 (1989)

12. C.A.Kelsey, F.A.Mettler, J.H.Christie, A.Williams, R.Rosenberg, "Comparison of Modulation Transfer Function (MTF) and contrast detail image evaluation tests", SPIE, 347,90 (1982)

13. R.P.Schwenker, "Signal-to-Noise Ratio, dynamic range and contrast sensitivity of radiographic imaging systems", SPIE, 419, 54-59 (1983)

14. R.Shaw and R.L.VanMetter, "The role of screen and film in determining the noise equivalent number of quanta recorded by a screen-film system," SPIE,535, 184 (1985)

15. M.E.Noz, C.Q.Magaire Jr., *Radiation Protection in the Radiology and Health Sciences,* Lea & Febiger, Philadelphia (1979)

16. W.J.MacIntyre, S.O.Fedoruk, C.C.Harris, D.E.Kuhl, and J.R.Mallard, "Sensitivity and Resolution in Radioisotope Scanning", *Nuclear Isotopes in Medicine & Biology*, 8, 99-146, (1969)

17. E.F.Gloyna and J.O.Ledbetter, *Principles of radiological health*, M.Dekker, New York, (1969)

18. R.Shaw, "The Role of Screen Parameters and Print-through in the Performance of film screen systems", pre-print, (1992)

19. D.Tody, "The Image Reduction and Analysis Facility (IRAF)", SPIE, 627, 733, (1986)

20. B.Whiting, Presentation at Center for Image Science in Rochester Institute of Technology. (1992)

21. E.Kelly-Fry, "The Rationale and Efficiency of Applying Multiple Image Technology for Breast Examination:X-ray mammography & ultrasound visualization", SPIE, 419, 31 (1983)

22. "KAF-4200 Specification Document", Eastman Kodak Company, (1990)

23. R.Shaw, "Advanced Principles and Techniques of Imaging Science", course notes for PMIG-703 (1990)

24. J.R.Janesick, T.Elliott, S.Collins, M.M.Blouke, J.Freeman, "Scientific Charge-coupled Devices", Optical Engineering, 26, 692 (1987)